Detection and analysis of thermokarst related landscape processes using temporally and spatially high-resolution Planet Cube Sat data

Master's thesis

Submitted in fulfillment of the requirements for the degree of

Master of Science (MSc)

at the Department of Geography

Paris-Lodron-University of Salzburg

Submitted by:

Wolfgang Senoner, BSc 1321152

wolfgang.senoner@stud.sbg.ac.at

Supervisor:

Univ.-Prof. Dr. Andreas Lang

Date of submission:

Salzburg, July 2019

STATUTORY DECLARATION

I declare that I have authored this thesis independently, that I have not used other than the declared sources / resources, and that I have explicitly marked all material which has been quoted either literally or by content from the used sources.

I am aware that the thesis in digital form can be examined for the use of unauthorized aid and to determine whether the thesis as a whole or parts incorporated in it may be deemed as plagiarism. For the comparison of my work with existing sources I agree that it shall be entered in a database where it shall also remain after examination, to enable comparison with future theses submitted.

This thesis was not previously presented to another examination board and has not been published.

July, 2019

……………………………….

(Date)

……………………………….

Wolfgang Senoner, BSc

(Signature)

Preface

Motivation

Since I was a little kid, I was fascinated by different landscape elements. Due to the fact I've already traveled a lot, these impressions have been reinforced. My journeys took me already to Australia, Indonesia, Singapore, Sri Lanka, Canada, multiple times the USA, Netherland Antilles, and many parts of Europe. There were also many exciting landscape processes to see, such as the sliding rocks in Racetrack Playa in Death Valley National park, volcanic eruption in Indonesia, different geological faults as well as the influence of glaciers on the landscape and many more. To understand all these processes, a geography study was just the right way to go. During my studies, I got to know different fieldwork methods. Particularly the data analysis was always very exciting for me. However, especially during my internship in Potsdam at the Alfred Wegener Institute, I gained exciting impressions of remote sensing methodology. This internship also led me to write this master's thesis in the field of remote sensing. There are many exciting topics and processes that can be explored in that field. Also, in the future, I would like to continue to work with remote sensing.

Acknowledgements

Abstract

This Master's thesis provides an overview of the methods to automatically detect different landscape processes in thermokarst areas. As the Arctic region is vulnerable to climate change, different developments lead to a fast-changing landscape. Especially three different processes are of interest: coastal erosion, retrogressive thaw slumps and thermokarst lakes. To detect the influence of these processes on the environment, different methods have been tested. As a basis for the evaluation Planet images were used. This data is acquired via nanosatellites with a resolution of 3 meters. Due to their small size and low cost, more than 200 active satellites are in the orbit monitoring the entire earth daily. With the help of a Python script, an automatic detection is possible, which leads to a classification afterwards. This is followed by an evaluation of the generated data. This data showed that the coast of Alaska is eroded at over 20 meters per year, the growth rate of thaw slumps in Noatak Valley exceed more than 25 meters per year. Surprisingly, thermokarst lakes in Siberia tend to be stable and no drainage could be detected.

Zusammenfassung

Diese Masterarbeit gibt einen Überblick über die Methoden zur automatischen Erkennung verschiedener Landschaftsprozesse in Thermokarstgebieten. Da die Arktis anfällig für den Klimawandel ist, führen unterschiedliche Entwicklungen zu einer sich schnell verändernden Landschaft. Von Interesse sind hier vor allem drei verschiedene Prozesse: Küstenerosion, retrograde Taurutschungen und Thermokarstseen. Um den Einfluss dieser Prozesse auf die Umwelt festzustellen, wurden verschiedene Methoden getestet. Als Grundlage für die Bewertung wurden Daten der Firma Planet verwendet. Diese Daten werden durch Nanosatelliten erfasst, und liefern eine Auflösung von 3 Metern. Aufgrund ihrer geringen Größe und niedrigen Kosten sind mehr als 200 aktive Satelliten in der Umlaufbahn, welche die gesamte Erde täglich abbilden. Mit Hilfe eines Python-Skripts wird eine automatische Erkennung ermöglicht, anschließend werden die Daten klassifiziert. Daran schließt eine Auswertung der generierten Daten an. Diese Daten zeigten, dass die Küste von Alaska über 20 Metern pro Jahr erodiert wird, die Wachstumsrate der Taurutschungen im Noatak Valley mehr als 25 Meter pro Jahr überschreitet. Überraschenderweise sind die Thermokarstseen in Sibirien stabil und es konnte keine Entwässerung festgestellt werden.

Detection and analysis of thermokarst related landscape processes
using temporally and spatially high-resolution Planet Cube Sat Data

Table of contents

Table of figures

1. Introduction

1.1. Scientific background

The Arctic region has developed to a hotspot when it comes to climate change (Dethloff et al., 2019). Temperatures in the Arctic are rising twice as quickly as the global average. This warming and its induced feedback processes are called the Arctic amplification. The mostly acknowledged instrument for Arctic amplification is the "insulation feedback". If the arctic sea remains free of ice in winter, a turbulent heat flux can be induced from the open sea surface. The heat flux is contributory for warming the lower troposphere (Kwang-Yul et al., 2016). The Arctic amplification is a representative attribute in the climate system. Evidence for the changing environment could be found in the Arctic because of an increased plant growth as well as thawing permafrost locally in Alaska and the Arctic (Serreze and Barry, 2011). The circum-Arctic region is mostly known for the occurrence of glaciers and sea ice, but also for permafrost. It is defined as ground that remains below 0°C for more than two years. Permafrost may contain of bedrock, sediment, soils, organic material and may or not may comprise ground ice (van Everdingen, 1998). It is a characteristic feature of areas not covered by ice-sheets and glaciers. It occurs in regions which are characterized by cold winters combined with low snow depth. A long-term negative annual heat energy balance of the land surface is the result. Roughly one quarter of the terrestrial area in the northern hemisphere is affected by permafrost (See Figure 1) (Zhang et al., 2000). Occurrence of permafrost reflects a negative heat balance at the ground surface. The thickness of permafrost is determined by a balance of internal heat gain with depth and heat loss from ground surface (French, 1976). The end of the last glacial maximum is also likely to be the maximum permafrost extent. It occurred under the coldest and driest climate conditions. Although this is not necessarily synchronous with the period of maximum ice volume in the northern hemisphere (Lindgren et al., 2016). The rising global annual mean air temperature of 2-3°C over the last decades led to an increase in ground temperature by 0.4 to 1.3°C in the upper part of permafrost. That in turn led to an intensification of cryogenic processes (Desyatkin et al., 2015). Land surface temperatures in Arctic regions are increasing twice as quickly as global temperatures. These warming temperatures lead to associated changes in land surface properties, especially in permafrost areas (Muster et al., 2015). The thermal regime of permafrost is very susceptible to changes in climatic conditions, especially in rising air temperatures (Smith et al., 2010,

Christiansen et al., 2010, Romanovsky et al., 2010). Even if the air temperature wouldn't rise more than 2°C until 2100 on a global scale, permafrost is going to degrade at significant areas. Thawing permafrost leads to serious changes for infrastructure, hydrological- and ecosystems (Biskaborn et al., 2019).
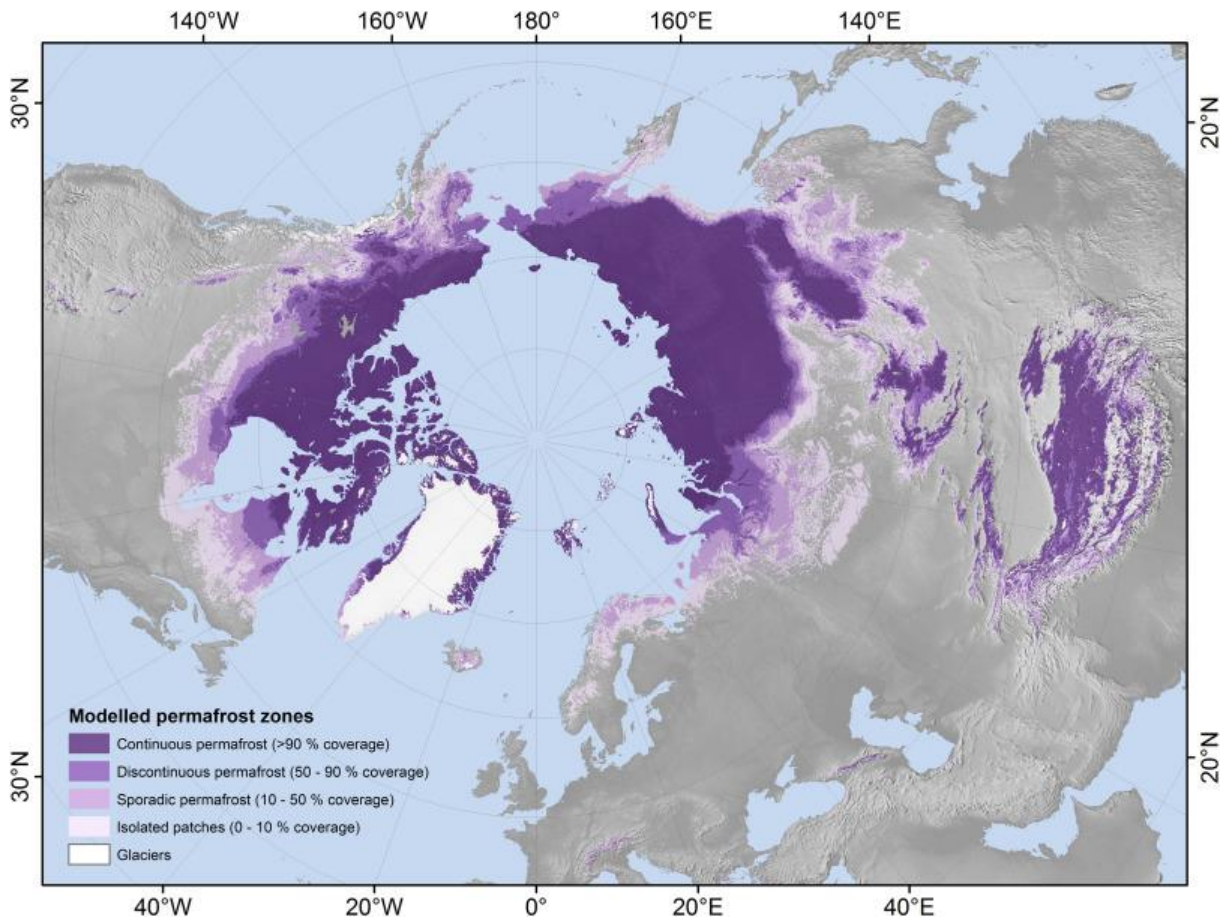
Figure 1: Permafrost distribution Northern Hemisphere (Obu et al., 2019)

Due to thawing ground ice the permafrost soil subsides and coastal- and lake shorelines erode. Because of the melting ground ice, surface wetting was observed, and new lakes and ponds have been formed. The thawing of ground ice may also lead to a changing environment due to lake drainage. Current climate projections are predicting more dramatic changes in land surface properties in the next decades, including spread of shrub and forest at the expense of Tundra. This is accompanied by albedo changes, which are expected to increase temperature changes over land (Muster et al., 2015). If ground ice in fine-grained sediments surpasses the pore space of the soil, melting of the permafrost can cause the surface to settle or liquefy. The amount and the type of ice is directly connected to the amount of settlement. The resulting irregular topography due to the melting of excessive ground ice and subsequent thaw settlement is called thermokarst (Jorgenson, 2013). The word "thermokarst" was introduced

by Ermolaev in 1932. Thermokarst, like most of the permafrost-related processes, have been first described by Russian scientists. In Russia more than 70% of the nationwide ground are affected by permafrost. In parts of central and eastern Siberia, roughly 40% of the surface have been affected by any thermokarst related landscape process at some time. Over a very long period (centuries to millennia) thermokarst processes can form wide depressions. Thermokarst is limited to areas underlain by permafrost. The essential condition for the development thermokarst is the occurrence of ground ice in close vicinity to the surface. Constant ground ice can only occur within permafrost bodies. Ground ice appears in pores, cavities, voids or other openings in soils and rocks. There are different forms, ground ice can occur, like lenses, wedges, veins, sheets, seems or as different crystals. For the development of thermokarst, two generalized types of ice can be considered: texture-forming ice and massive ice. The development of thermokarst is linked to seasonal thaw propagation in ice-rich layers of the transition zone and deep permafrost. Although the correlation between climate changes and the development of thermokarst is not straightforward. The development of thermokarst in Siberia over the last 50 years related primarily on the intensification of precipitation rather than changing air temperature. Thermokarst can advance on a local scale in stable cold climatic conditions. Vegetation and soil disturbances are important factors contributing to thermokarst. Removal of vegetation either through natural or human activities leads to increasing degradation of the permafrost in the active layer and is in most cases irreversible. Two groups of thaw processes can be linked to thermokarst: erosional processes and processes related to ground ice (Shiklomanov and Nelson, 2013). Thermokarst terrain shows a pitted relief shaped from the melting ground ice. Processes related to thermokarst are usually only considered with respect to permafrost topography, soil displacement due to melting of seasonal frost is not included. Thermokarst terrain and their landforms can be found in permafrost regions where ground ice is exposed or melted. These features are uncommon in bedrock areas, but they may occur locally in depressions where a sediment cover, including ground ice, has accumulated. The volume of water released as ice melts is usually higher than the saturation water content, resulting in rising pore-water pressure. The union of thawed soil in flat terrain leads to subsidence of the ground and an undulating topography as the rate and extent of thawing is spatially variable. The variability is mainly due to the heterogeneous distribution of ground ice. In steeper terrain, high pore-water pressure, leads to a decrease in effective stress as well as loss of soil

strength, so slopes may fail. In permafrost terrain landslides are common (Burn, 2013). Ice rich permafrost formed enormously in Siberia at the alteration from Pleistocene to Holocene. Since then, only minor changes to the landscape occurred (Romanovskii et al., 2004). Beside the theory of unidirectional thermokarst development, containing initiation, expansion, drainage as well as termination of thermokarst activity which leads to a steady and modern thermokarst landscape, thermokarst has always been considered as a very active process. The conception of a thaw lake cycle which has been recurring numerous times throughout the Holocene has been anticipated (Hinkel et al., 2003). This perception designates a secondary thermokarst activity in basins which are already drained after adequate ice degradation, although significant evidence is missing that numerous full thaw cycles have befallen during Holocene in arctic tundra landscapes (Jorgenson and Shur, 2007). There are great variances among the settings in which the potential and impact of emerging thermokarst in undisturbed and ice rich late-Pleistocene deposits and these in older generation thermokarst basins(Kessler et al., 2012). Though, there is still a gap in our information about the development of these permafrost degraded landforms during the Holocene(Morgenstern et al., 2013). To detect changes in permafrost/thermokarst landscapes, remote sensing systems are being used. The emerging number of observation systems cover a wide range of temporal and spatial scales (Jorgenson and Grosse, 2016). Remote sensing cannot directly reflect permafrost absence or occurrence, but the acquired data by remote sensing helps to complement collected data from field trips. Among other things, different models for the distribution of permafrost can be created within the scope of different remote sensing systems (Shi et al., 2018). Furthermore, automatic and semi-automatic methods, based on remote sensing images, have been developed. Mostly by using different machine learning algorithms. Although it is very challenging to automatically detect different thermokarst landscape forms (Huang et al., 2018).

1.1.1. Related landscape processes

Regional landscape dynamics are driven by permafrost-related processes in the Arctic terrestrial system. To predict future dynamics a better understanding of these processes is necessary. Permafrost warming, and thawing has been observed for several decades. A degradation of permafrost dominated landscapes influences different areas of the ecosystem like hydrology, ecology, ground thermal regime as well as biogeochemical cycles (Lenz et al., 2016). For this study three different types of related landscapes processes have been

identified, as these provide a good overview of the current situation in arctic regions. Rapid coastal erosion in the Arctic indicates changing climate. Although the Beaufort Sea in Alaska is frozen for 8-9 months per year, rates of erosion are around 2-4 myr^{-1} being one of the highest in the world (Jorgenson and Brown, 2005). Due to the steady increasing temperatures fundamental changes in biological as well as physical processes occur. These processes modify permafrost landscapes (Cunliffe et al., 2019). Coastal erosion playing a serious part in long-term evolution of permafrost shorelines (Barnhart et al., 2014). Another related landscape process are retrogressive thaw slumps. Disturbance in terrain may lead to changes in the ground thermal regime, melting ground ice, as well as soil subsidence or enhanced erosion. Amongst the most active geomorphological features in permafrost areas are retrogressive thaw slumps. Usually they are found along the banks of northern rivers as well as lakes. The slumps stabilize their self, when the exposed ground ice of the retreating headwall is completely thawed or covered by debris (Burn and Friele, 1989). Retrogressive thaw slumps can reach a surface of several hectares (Kokelj et al., 2009). Due to recent climate changes it is assumed that changing landscape processes are going to increase (Lacelle et al., 2010). The evolution of thermokarst lakes is the final related process. These lakes are a typical landscape part in Arctic regions. Even little disturbances can induce thermokarst related processes which are able to create lakes. Water is gathering in these depressions and thaws the permafrost underneath. As long as the thaw process is continuing, the pond expends(Kääb and Haeberli, 2001). Thermokarst lakes were formed during the warmer Holocene climate, when the ice wedges started to thaw. These lakes enlarge till a drainage channel developed. The draining lake led to lower water level. If the lakes drain completely, the remaining organic matter, could freeze again and form permafrost (Walter et al., 2007).

Coastal erosion

Eroding Arctic coastlines reflect the multifaceted interaction between climate, geomorphology, geology in which soil properties related to permafrost are subjected to thermal as well as mechanical instability (Aré, 1988). Arctic coast retreat with average rates of 1 – 2m/a. Always depending on local climatic and

Figure 2: Arctic map of coastal erosion rates (edited from Lantuit, 2012)

permafrost conditions (Novikova et al., 2018). Compare Figure 2 for erosion rates across the Arctic.

Permafrost coasts are highly dynamic landscapes. Roughly two third of Arctic coastlines are unlithified but coalesced by permafrost. Upon thaw, many of the Arctic shorelines are affected by high erosion rates. There are large impacts on ecological and socio-economic dimensions of coastal systems due to erosion. Coastal erosion also threatens infrastructure and settlements along the coast. Due to an increasing air temperature, higher permafrost and water temperatures occur, along with a decreasing sea ice extent as well as deeper thawing depths of soils. All these features are affecting coastal erosion rates (Irrgang et al., 2018).

Rates of coastal erosion in the Arctic vary temporally and spatially. Global warming leads to increasing coastal erosion rates (Aleksyutina et al., 2018). The variability is based on different factors like hydrometeorology, coastal morphology as well as permafrost features of the coastal sediments (Belova, 2018). The distinctive feature of polar coasts is the occurrence of a variation of ice types on and ground ice below the earth surface. The impact of hydrometeorological conditions influences the development of coastal thermoactive erosion, as well as thermal and wave energy, both of which are related to the extent and duration of sea ice. Clastic material enters the near-shore zone because of coastal erosion, where it is deposited, reworked and transported. As ground ice occupies a large proportion of the land's

volume (above and below sea level), a smaller quantity of material is detached by wave action after thaw than along ice-free coastlines and high rates of coastline retreat are the result. Typically, thawed material is being eroded, rather than permafrost. Coastal thermo-erosion comprises two related processes, which are working temporally and quantitatively different together. Thermo-denudation (TD) contains of the thawing of exposed permafrost, the propagation of a retreating headwall upslope or inland as well as the transport of material downward to the bottom. Everything under the influence of insolation and heat flux on the slope. Thermo-abrasion (TA) is determined as a combination of mechanical and thermal energy of sea water at water level. Although there are temporal disparities in their intensity, both processes are interconnected, as the Thermo-denudation becomes inactive after the Thermo-abrasion has come to a standstill (Günther et al., 2015).

Retrogressive thaw slumps

Another effect due to increasing temperatures is the rate of permafrost degradation and thermokarst. In ice-rich terrain retrogressive thaw slumps are one of the most dynamic thermokarst features(Brooker et al., 2014). Retrogressive thaw slumping is an active form of thermokarst slope disturbance, which pairs thermal and geomorphic processes to quickly degrade ice-rich permafrost. Slope morphology can be modified, and a large amount of thawed material can be transported downslope to lakes, valley bottoms and coastal zones. Thaw slumps can be the most dominant driver of landscape changes in ice-rich permafrost regions (Kokelj et al., 2015). Retrogressive thaw slumps are having three main elements (see Figure 3): 1.) A vertical or sub-vertical headwall, consisting mostly of the active-layer along with ice-poor organic or non-organic material. 2.) A head scarp, with varying angles between 20° to 50°. It retreats because of the ablation of ice-rich material due to sensible heat fluxes and solar radiation. 3.) The slump floor, which consist of unsolidified mudflow and flow deposits that enlarge in a lobe pattern at the toe of the slump. Often a massive amount of ice (15 – 20m) is exposed in the head wall of the retrogressive thaw slump. Depending on the

fragments of sediments accumulating at the base of the headwall (Lantuit and Pollard, 2008).
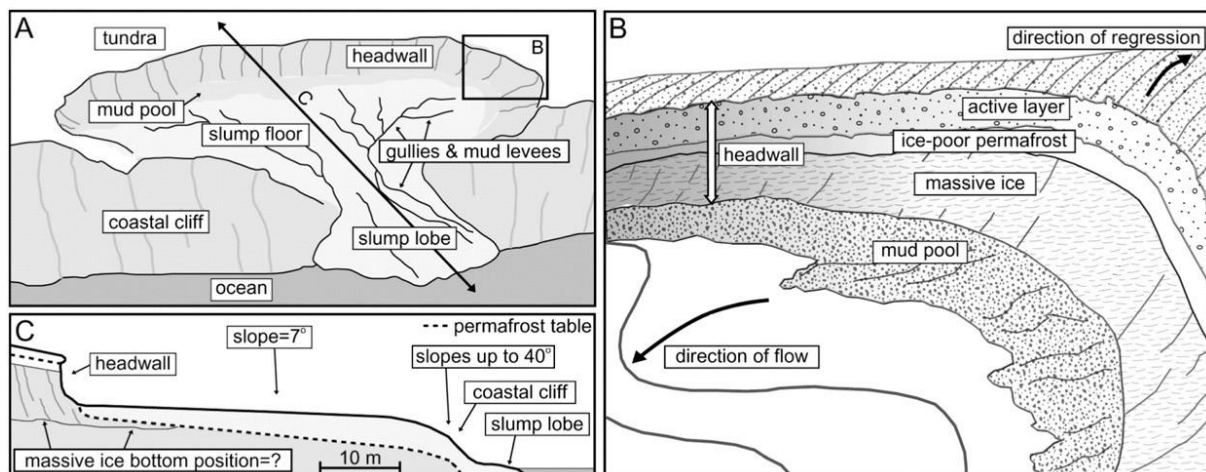
Figure 3: Conceptual scheme retrogressive thaw slump (Lantuit & Pollard, 2008)

Retrogressive thaw slumps keep on growing as long as the ice-rich permafrost in the headwall remains exposed or the supply of ground ice is exhausted (Lacelle et al., 2015). Thaw slumps usually are initiated by a detachment slide, which removes soil from the active layer and exposes permafrost to swift melting. After the initial degradation, the thawed material usually enlarges laterally upslope along the exposed headwall. Many slumps are short lived and become stable after 30-50 summers (Jorgenson, 2013). If the ice-rich material though becomes exposed, due to different possibilities, the slump may be reactivated. There have been maybe up to three periods of thaw slump activities during the Holocene: near the end of the early Holocene warm interval, during mid-Holocene as well as the Little Ice Age (Lantuit et al., 2012). Different geomorphic processes can operate during the formation of a thaw slump, this includes falling and slumping of sediments as well as sliding and flowing of thawed material (Millar, 2013). Retrogressive thaw slumps are polycyclic in nature and separate disturbances are frequently encompassed of old, recently stabilized and active scar area, affecting the terrain extensively. The effect on terrain stability is also relevant for planning of linear infrastructure such as oil and gas pipelines (Lantz and Kokelj, 2008). Due to these multiple processes, different terminology is used in the literature. Though, retrogressive thaw slump is the preferred term. Initial failure can be due to coastal wave erosion or high river flows during intense rainfalls. As well because of forest fires and of course human impact. Retrogressive thaw slumps develop if ice-rich permafrost thaws under unconsolidated soil. The rate of retreat depends strongly on the ground-ice content. In coastal regions retreat rates up to 11m/a have been observed. In non-coastal regions rates are up to 5m/a.

Higher rates at coasts can occur due to wave action (Millar, 2013). Thaw slumps are mainly found along lake and river shorelines, coastlines and hillslopes. A variety of mechanisms that expose ice-rich permafrost are responsible for the occurrence of slumps. Contrasting landslides in non-permafrost environments, upslope ablation of the slump headwall can endure for many years till the ground ice supply is bushed or the headwall is covered by slumped material. If a part of the headwall remains inactive for a longer period, sediments on the adjacent slump floor begin to dry. This can lead to growing vegetation in that area. Due to infrequent coverage provided by aerial photographs, the relation between the evolution of thaw slumps and climate or other environmental or landscape factors are restricted often to decadal or multi-decadal timescales (Brooker et al., 2014). Thaw slumps also have a significant impact on the formation and development of thermokarst lakes. As ground subsidence as well as tipping of trees because of permafrost degradation, followed by immersion of vegetation and formation of thaw slumps along the lakeshore (Wang et al., 2018). Malone et al. (2013) investigated thaw slumps and found evidence that these features can degrade up to 10m of permafrost and affect a watershed stream widely.

Thermokarst lakes

Study by Lehner and Döll (2004) revealed that the highest concentration of lakes in de-glaciated areas lies between 50° and 70° Northern latitude. Their dispersal can be principally explained by prior glaciation, presence of peatland as well as the occurrence of ice-rich permafrost (Nitze et al., 2017). Thermokarst lakes are defined as lakes that inhabit generally closed depressions formed by the settlement of ground ice following by thawing of ice-rich permafrost or melting of massive ice cores (van Everdingen, 1998). They form in areas where excess ground-ice is present, and the content of ice is more than 30 percent by volume. Thermokarst lakes as well as drained lake basins are prevalent in Arctic and sub-arctic permafrost lowlands. The formation of thermokarst lakes is a main mode of permafrost degradation and is related to different processes like surface disturbances, subsequent melting of ground ice, surface subsidence, water impoundment. Thermokarst lakes typically have unique limnological, morphological as well as biochemical characteristics which are in close relation to cold climate conditions and permafrost properties(Grosse et al., 2013). There is also a tendency towards complete or partial draining through permafrost degradation and erosion. Thermokarst lake formation and its growth affords a mechanism for deep and rapid

Ice-rich permafrost with ice wedges

Water (lake)

Lake talik

Trees

Permafrost table

Terrain surface
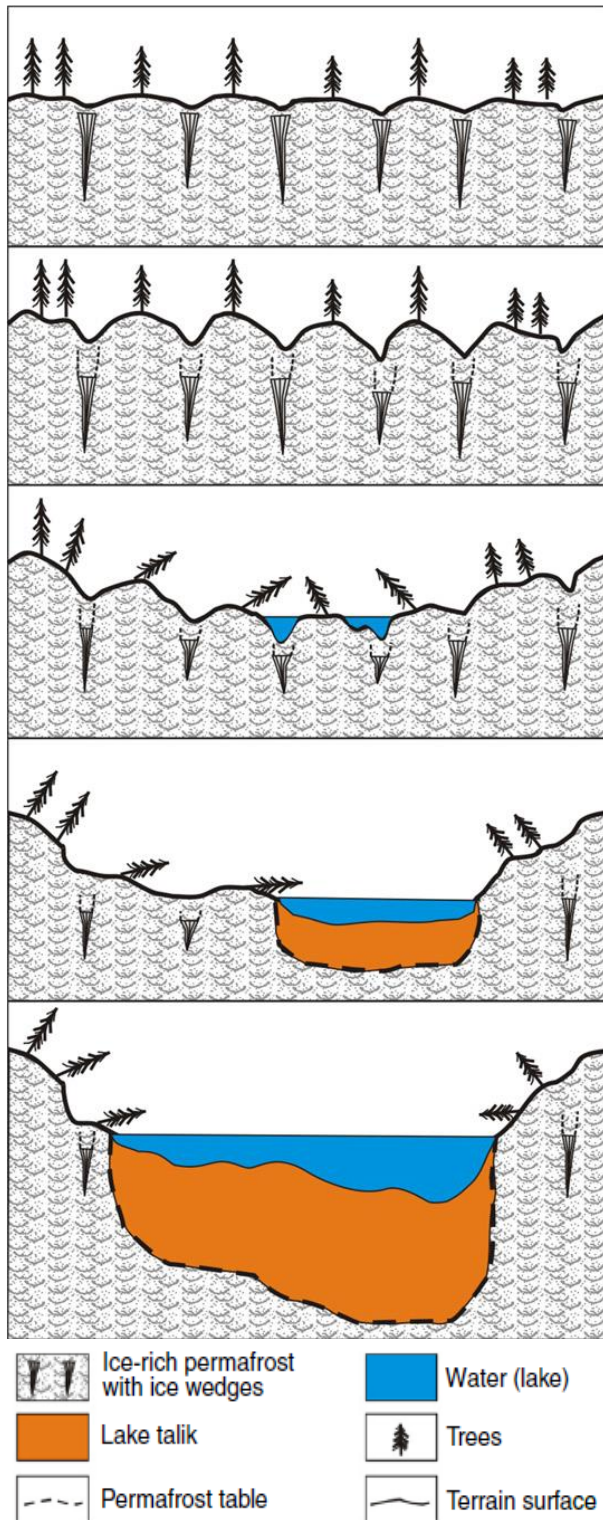
Figure 4: Thermokarst lakes development (Grosse et al., 2013)

permafrost degradation. The occurrence of thermokarst lakes represents a local disturbance to the ground ice thermal regime (Jorgenson et al., 2010). These lakes have also been identified as an important source of atmospheric greenhouse gases like methane and carbon (Zimov et al., 1997, Kling et al., 1991). Thermokarst lakes are also used for human purposes as a residential fresh water source in Arctic regions, as an industrial water resource as well as fishing and hunting grounds (Alessa et al., 2008). In Arctic regions the occurrence of thermokarst lakes is mostly controlled by the presences of permafrost and the glacial history (Smith et al., 2007). The distribution of thermokarst lakes is dominant in permafrost dominated regions with a moderate to high ground-ice content and as well as a thick sediment cover. The development of thermokarst lakes can be seen in Figure 4. Long term heat flux of the thermokarst lake, allows thawing of the permafrost and melting of ground-ice underneath the water body. The result is volume loss, sediment compaction, subsidence as well as growth of lake depth and volume. Another important process of thermokarst lake development is the formation of talik underneath a lake. The annual heat flux shows that the water body receives heat energy from the atmosphere in summer time which is then dissipated in the lake and partially transferred to surrounding and underlying sediments of the talik. In autumn and early winter season, the lakes are cooling rapidly while the upper part of the talik is warmer than

the lake water because of the late summer warmth pulse is still present in the talik sediment. In winter, thermokarst lakes emit heat into atmosphere, although there is an ice cover, while heat transfer into the talik continues to expand by transferring heat into permafrost. Heat fluxes always point from the talik into the permafrost. Thermokarst lakes also tend to grow laterally due to thermal and mechanical abrasion. The water storage in thermokarst lakes is supplied by snowmelt in spring, rainfall in summer as well as the contribution of ground-ice. Thermokarst lakes develop and expend due to the degradation of surface permafrost (Czudek and Demek, 1970, Grosse et al., 2013). Though the water balance of thermokarst lakes are affected by climate dynamics, another important influence is that they tend to expend in depth as well as laterally. This may lead to lake drainage. Sometimes, the drainage can be described as a catastrophic event, as rapid deepening and widening of the drainage channel can occur within several hours. Draining can also occur as a fact of coastal erosion. Although, the most frequent cause is the drainage due to ice-wedge degradation (Grosse et al., 2013). Thermokarst lakes are usually small, being under 10km in diameter. In numerous regions, various drained lake basins have been observed, often with several generations superimposed, indicating episodic or constant lake formation and drainage over many centuries. In addition, they are possibly a substantial source for methane (Edwards et al., 2016).

1.1.2. Planet Cube Sat

Planet Labs Inc.'s aim is to provide information about the changing planet as well as humanitarian applications, with universal data access. One of the biggest advantages of Planet satellites is their daily monitoring of the entire earth. Combined with a 3m resolution makes it a perfect source for constant process monitoring. Satellites are pointing always at towards nadir and the cameras are always on, if the satellite is flying over land. To monitor the Earth on a daily base, a minimum of 105 satellites is required. To operate flocks of satellites in this size presents unique challenges. It is highly necessary to track each satellite accurately. In-house differential drag control technology was required as there is no onboard propulsion. Image files are being downloaded from a satellite via a high-bandwidth X-band link. This requires pointing errors from the ground station antenna must not exceed more than 0.2° (Foster et al., 2015). Planet Labs Inc. operates PlanetScope (PS), RapidEye (RE) as well as SkySat (SS) Earth-imaging constellations. Image data is being collected and processed in different formats, adopted for different use cases. Image mapping, deep learning, disaster response,

precision agriculture and temporal image analytics to gain information for different products. PlanetScope imagery is captured as a nonstop single strip frame known as scenes. These scenes can be either acquired as a single RGB (red, green, blue) frame or a split frame, half RGB and half NIR (near infrared), always depending on the capability of the satellite. Planet offers three different product types: Basic Scene Product, Ortho Scene Product and Ortho Tile Product. Basic Scene is a scaled Top of Atmosphere Radiance and sensor-corrected product. This scene is for users with a wider knowledge in image processing and geometric correction capabilities as it is not orthorectified and corrected for terrain distortions. Ortho scene image is the original frame of the satellite, with additional post processing already applied. Ortho Tile scenes are orthorectified multiple times in a single strip which has been merged and then divided according to a defined grid. PlanetScope satellite constellation involves individual satellites, launched in groups multiple times. So called flocks or doves. Therefore, capability and quantity of the image products are constantly improving. Each Planet CubeSat has the following dimensions: 10cm x 10 cm x 30cm. All PlanetScope satellite can image the entire earth once a day. This equals a daily data collection of roughly 150 million km² per day. Different orbits are flown, the constellation overview can be seen in Table 1 (Planet Labs Inc., 2018). The main component is a telescope and a CCD area array sensor (charge-coupled-device). The power supply is secured through solar panels, a GNSS (Global Navigation Satellite System) receiver is responsible for satellite position and a star tracker for the satellite orientation. The ground resolution along with the size of the scene varies with different flying height as well as the satellite generation. As in Table 1 can be seen, CubeSats flying a near-polar orbit with an inclination of 98°. The altitude is about 475km. This near-polar orbit guarantees a sun-synchronous coverage (Kääb et al., 2017).

Table 1: PlanetScope Constellation and Sensor Specification (Planet Labs Inc., 2018)

CONSTELLATION OVERVIEW: PLANETSCOPE

Mission Characteristics	International Space Station Orbit		Sun-synchronous Orbit	
Orbit Altitude (reference)	400 km (51.6° inclination)		475 km (~98° inclination)	
Max/Min Latitude Coverage	±52° (depending on season)		±81.5° (depending on season)	
Equator Crossing Time	Variable		9:30 - 11:30 am (local solar time)	
Sensor Type	Three-band frame Imager or four-band frame Imager with a split-frame NIR filter			
Spectral Bands	Blue	Green	Red	NIR
	455 – 515 nm	500 – 590 nm	590 – 670 nm	780 – 860 nm
Ground Sample Distance (nadir)	3.0 m (approximate)		3.5 m - 4 m depending on flock	
Frame Size	20 km x 12 km (approximate)		24.6 km x 16.4 km (approximate)	
Maximum Image Strip per orbit	8,100 km^2		20,000 km^2	
Revisit Time	Variable		Daily at nadir (early 2017)	
Image Capture Capacity	Variable		340 million km^2/day	
Camera Dynamic Range	12-bit		12-bit	

For this study PlanetScope Analytic Ortho Tile product was used. Analytic images are calibrated multispectral imagery products, which have been processed, allowing users to derive information products for data science and analytics (Planet Labs Inc., 2018). As CubeSats offering a high spatial resolution (~3m) as well as temporal, they open new possibilities e.g. for temporally dynamic hydrological processes from space. CubeSat can overcome the compromise between high spatial and high temporal resolution by arranging them in multi-satellite constellations. Since 2013 more than 281 CubeSats have been built and launched. 148 of these satellites are in sun-synchronous orbit (see Table 1). The daily imaging of the entire earth offers a huge potential to evaluate different processes (Cooley et al., 2017). CubeSats in general, reducing the cost and complexity of development and launch, compared to traditional satellite systems with redundant systems. There is also a lower impact by small satellites from individual failures. Planet's flock of CubeSat satellites is the largest assemblage of commercial Earth imaging spacecraft. This results in a daily revisit time (Poghosyan and Golkar, 2017). It offers many different opportunities in various fields like: agriculture, water resource planning, surface water and its changes, flood monitoring, coastal erosion as well as land cover and land use changes (McCabe et al., 2017). Another field is disaster management in remote areas. Nanosatellites are important as they collect information over large areas in a short period of time, with a high resolution (Santilli et al., 2018). Compared to Planet traditional single-source satellite missions are cost intense and physically constrained in terms of spatial resolution and of course the revisit time. Landsat for instance offers partly high-quality sensors, high signal to noise ratio.

Though, the 16-day revisit cycle over the equator is a major limitation for applications which require surface conditions information more often. In Arctic regions the revisit cycle is shorter. Sentinel 2 satellites are having a five-day revisit capability. However, cheaper Planet sensors do not match the signal to noise ratio, radiometric performance, cross-sensor consistency and the spectral enhancements of the traditional satellite missions. Additionally, the lack of at-sensor radiance conversions as well as the atmospheric corrections of the RGB image are affecting the interpretation and time and space consistency of any time-series data (Houborg and McCabe, 2016). Despite all these advantages of Planet, there is one disadvantage. Landsat and Sentinel data are available free with no additional costs. The Planet researcher license is also free of charge, but you have to apply for it and without any scientific reason your access to their data could be denied.

1.2.   Hypothesis

These different processes and their impact on different local systems mentioned above led to the following research questions:

- Do highly spatial and temporal resolved Planet cube-sat data have the potential to detect and quantify thermokarst related landscape dynamics?

- Can the occurrence and sub-annual temporal and spatial patterns of these detected thermokarst features be analyzed by a machine-learning algorithm?

- How do the Planet cube-sat derived thermokarst feature datasets compare to existing data products based on lower-resolution Landsat data?

2. Study areas

1) Noatak Valley, AK: Retrogressive thaw slumps
2) Drew Point, AK: Coastal erosion
3) Yakutia, Siberia: Thermokarst lakes
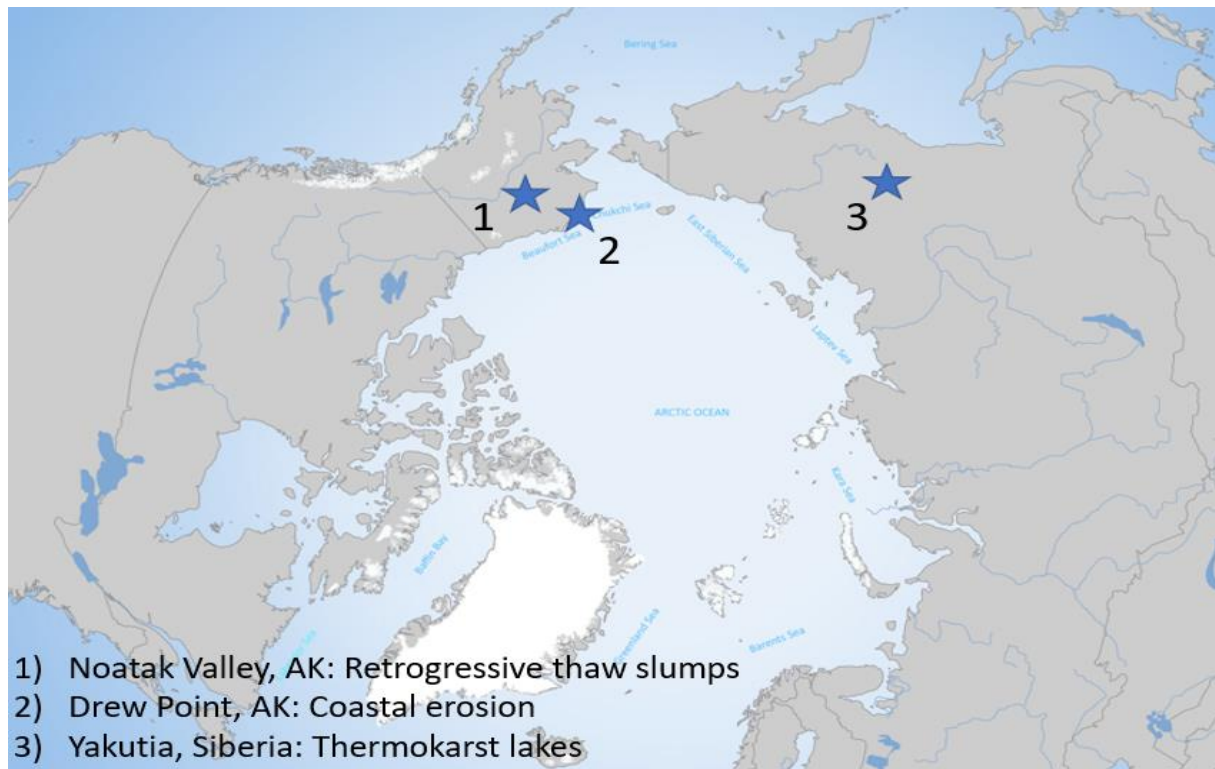
Figure 5: Study areas including related processes (edited from: https://www.thearcticinstitute.org/wp-content/uploads/2016/07/Arctic-Ocean-with-labels-high-res.jpg)

The study areas for this thesis are illustrated in the Figure (Fig. 5) above.

2.1. Alaska

The North Slope of Alaska is specifically vulnerable to climate change, as higher latitudes are influenced by positive snow- and sea ice atmosphere feedback under warming conditions and the dynamics of iced sea- and landscapes are strongly determined by thermal regime. Rising temperatures lead to deeper soil active layer above the permafrost (Kittel et al., 2011). The State of Alaska is underlain by permafrost up to 80 percent. Of these 80 percent, continuous permafrost makes up 29 percent, discontinuous 35 percent, sporadic 8 percent as well as 8 percent isolated permafrost. 15 percent of the State is under no influence of permafrost, glaciers and ice sheets occupy 4 percent, and 1 percent are large water bodies (Jorgenson et al., 2008). A lot of this permafrost is warm, within a couple degrees of thawing (Osterkamp et al., 2009). It is assumed that the temperatures in the Arctic are rising faster, compared with other parts of the world. Especially in the area north of 60°N latitude it will be two times as fast as the worldwide average (Betts and Kane, 2014). On a global scale, temperatures were rising since the late 1880s (Hansen and Lebedeff, 1987).

In Alaska the temperatures continued to rise until about 1940. The third quarter of the century was cooler than before. This trend continued until the 1970s as the temperatures began to rise sharply. The change of temperature in Alaska is highly correlated with the changing temperatures in Alaska's permafrost regions. The annual mean temperature after 1977 was rising about 1°C to 2°C (Osterkamp and Romanovsky, 1999). These changing climatic conditions over the past century caused permafrost to warm. The southern boundary of permafrost has moved further north. Reports of thawing permafrost and thermokarst terrain are increasing as well as discontinuous permafrost is also thawing from the bottom at different sites. Thawing proceeds from top downward, eventually also from bottom upward. Rates can vary from 10cm/a at the surface to less than 2cm/a at the base (Osterkamp, 2005).

2.1.1. Drew Point
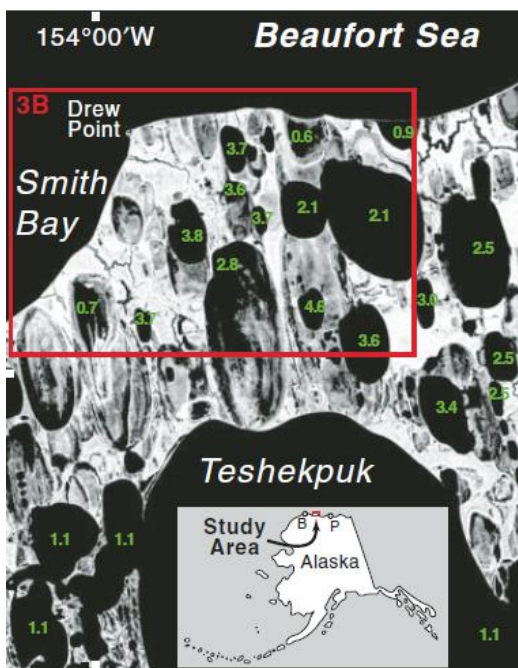
Figure 6: Drew Point, Alaska (Mars & Houseknecht, 2007)

Coastal erosion along the Beaufort Sea coast, has received extensive attention. Especially at Drew Point which is located within the National Petroleum Reserve in Alaska, north of Teshekpuk Lake (See Figure 6)(Mars and Houseknecht, 2007). Erosion rates at Drew Point are among the highest in the world (Jones et al., 2009). Mean annual erosion in 2007 at Drew Point was around 17 meters (Arp et al., 2010). Which was also observed by using remote sensing methods(Jones et al., 2018b). Long-term observations showing the average erosion along the Alaska Beaufort Sea is around 2.5m/a, with higher rates in the western areas (3.0 – 5.4m/a) compared to lower rates in eastern areas (1.0 – 1.4m/a) (Jones et al., 2008). The Beaufort Sea is ice-free between three and four month a year. In this short period the whole coastal erosion occurs. The main reason for the erosion is thermal abrasion (Jones et al., 2009). Sediment of this coastal-plain was deposited during Quaternary sea-level high stands, including fine, low relief sandy beach ridges detached by wider areas of lower lying silty marine deposits (Wobus et al., 2011). Large areas of the coastal plain are covered by thermokarst depressions. The area is surrounded by Tundra. The permafrost reaches a thickness of more than 250 meters. The soil in the first 5m below the surface consists of 75% ice and 25% sediment.

Early studies showing that the coastal erosion exceeds up to 20 meters per year of shoreline retreat. Coastal shoreline consists of high permafrost-bluffs (2-6m). The main process of coastal erosion is wave undercutting, this leads to permafrost block collapse. Beaches are poorly developed or absent along the coast line because of the predominance of permafrost. The wave energy is uncurbed on the permafrost-bluffs. The undercut blocks are falling directly in to the sea. These permafrost blocks thaw quickly in salt water due to convective heat loss, and wave action suspends and transports muddy sediment offshore (Mars and Houseknecht, 2007).

2.1.2. Noatak Valley

Noatak valley is located in Northern Alaska. As Figure 7 shows, the study site is within a hilly surrounding. Many retrogressive thaw slumps can be found here.
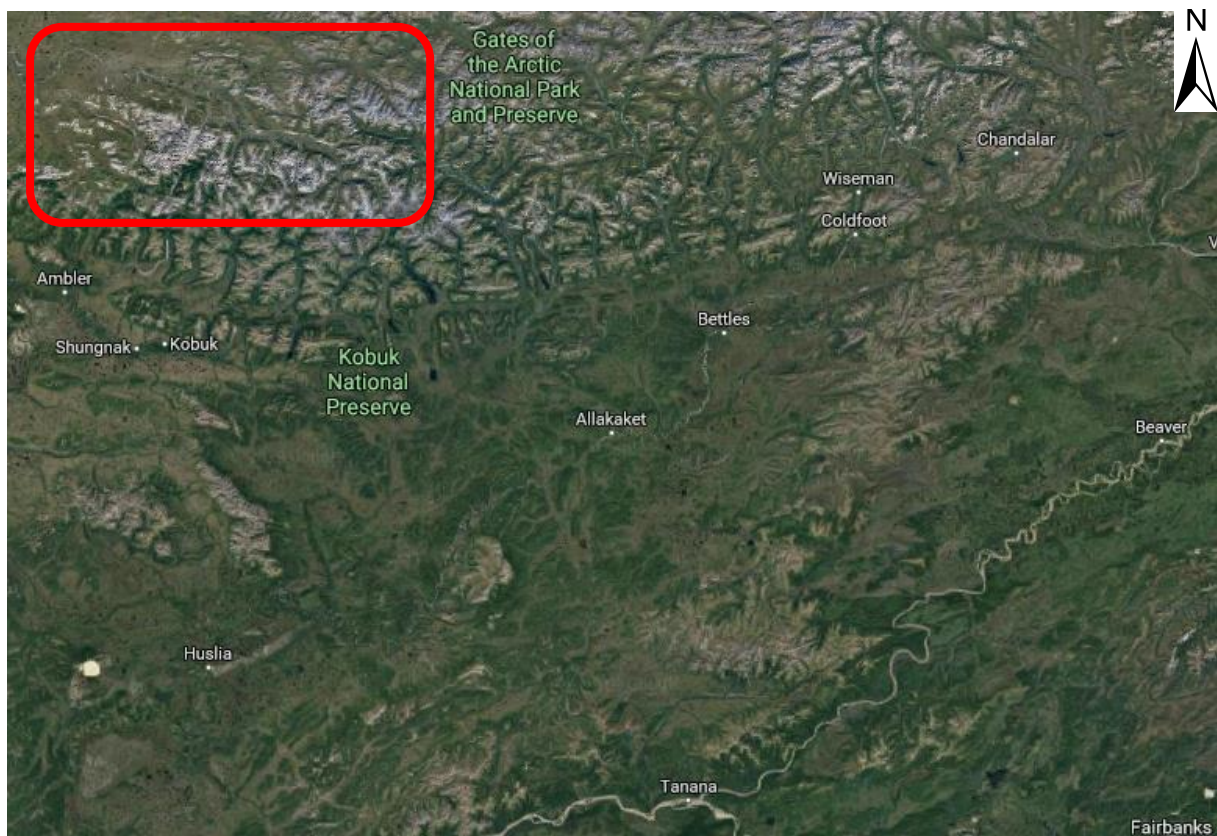
Figure 7: Study site Noatak Valley, Alaska (Screenshot Google Maps)

The Noatak basin is surrounded by mountains of western Brooks Range. Evidence of five major glacial advances were found (Hamilton, 2001). This is a region of continuous permafrost and arctic tundra vegetation. During the late Pleistocene this area was glaciated. The detected thaw slumps are mostly in deposits from Itkillik I and II glaciations. Itkillik II stage is coincided with the last worldwide glacial maximum (marine isotope stage II).

Glacial ice from these two advances has been detected in escarpment of retrogressive thaw slumps. The thaw season (daily mean temperatures above 0°C) is usually between mid-May through mid-September. Mean permafrost temperatures in study area are usually between -4°C to -7°C. The thickness of the active-layer is approximately 50cm. The annual mean precipitation June-August was 129mm (Swanson and Nolan, 2018). There is no climate station within the study area. To estimate climatic conditions, interpolation is used (Edwards et al., 2003).

2.2. Siberia – Yakutsk Area

Central Yakutia is within the zone of continuous permafrost. Depths of the frozen soil can reach some hundred meters. In grassland areas the active layer reaches a depth of 2 meters, below forest 1 meter (Ulrich et al., 2017a). Age-depth modelling using ^{14}C ages showing high rates of thermokarst sedimentation in Central Yakutia. During mid-Holocene for a time span of about 900 years (~ 6750 and 5870 cal. yr. BP). In total, three different stages could be detected (Ulrich et al., 2017b). Global climate warming impacts the natural environment, especially in permafrost regions. The region around Yakutia has severe, extremely continental climate with long winters between 7 and 8 months, and short summers with 3 to 4 months. Mean annual temperatures are between -6°C to -14°C. January mean temperatures range from -29°C to -48°C, in July temperatures are +12°C to +19°C. Record low temperature was -72°C, record high is +38°C. Mean annual precipitation is between 180mm to 680mm. Nearly four fifths of the region is underlain by continuous permafrost (with thickness up to 400 m). In the Vilyuy River Basin, the thickest permafrost can be found, with a depth of 1500m. Permafrost is absent in these regions below rivers and lakes. Permafrost formation in eastern Siberia began 2.5 – 3 Ma ago. Since this time, regional permafrost has undergone numerous changes with warmer and colder phases. Last glaciation occurred 12 – 25 ka ago. Spatial variations in permafrost temperatures, as well as the thickness of the active layer are mainly controlled by the landscape conditions. Generally, thickness of the active layer and ground temperatures decrease with increasing latitude (Desyatkin et al., 2015). Due to the high vulnerability of permafrost with respect to climatic changes extensive degradation can occur (Séjourné et al., 2015). Thermokarst affects local ecology, geomorphology, hydrology as well as the local climate. Remote sensing images show that thermokarst lakes can be indicators of a changing water balance (Morgenstern et al., 2011). Nearly all the lakes, located in Central Yakutia, have a thermokarst origin.

Their formation began about 11 thousand years ago. Cold and dry climate conditions were followed by warmer and wetter conditions. Warm and wet conditions were leading to lake expansion as colder and drier phases led to a lake retreat (Zakharova et al., 2018). As mentioned by Tarasenko (2013) atmospheric precipitation is one of the main sources of water recharge for most of the lakes in Central Yakutia. Lake areas were constantly increasing over the 1976-2000. Due to warmer and wetter weather since the 2000's lake area in Central Yakutia increased by more than 48% in the period of 1999-2014 (Nitze et al., 2017). Siberian thermokarst lakes were intensively studied during Soviet time as they are an important source for freshwater as well as agricultural purposes (Pestryakova et al., 2012).

3. Methodology and data
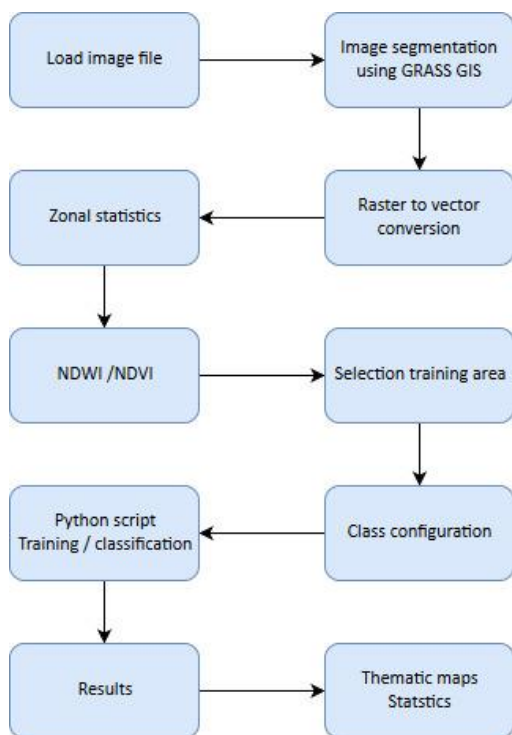
To detect and analyze landscape processes in Arctic regions, different steps were taken to accomplish these goals. As shown in the flowchart (Figure 8), the first important step is the image segmentation, as this is the base for the further detection. Zonal statistics, NDWI as well as NDVI need to be added to the shapefile ahead of the selection of the training data. The selected training data must encompass all existing classes, as they need to be defined when using the Python script. After the script is completed, the final step is the analysis of the results. Care was taken to standardize all steps as far as possible for all study areas. For Drew Point and Central Yakutia, the same script was used, Noatak Valley script differs slightly of these two.

Figure 8: Flowchart

3.1. Data acquisition

Data for this study was acquired using the Planet API downloader, following the instructions from an online tutorial (https://developers.planet.com/planetschool/downloading-imagery/). Here basic instructions are given, which needed to be adapted fitting the requirements of this

study. For this thesis, PlanetScope Analytic Ortho Tiles were used. These images are orthorectified, are already preprocessed, distortion is removed, as well as radiometric corrections are applied. The used images for this thesis can be found in the Annex.

3.2. Image segmentation and region growing algorithm

The task of image segmentation is extracting one or more objects of interest among many others in an image, based on minimal user input (Jumaat and Ke, 2019). The aim is to partition an image file into regions which are not overlapping. The definition of a region is a homogenous group of connected pixels with respect to a chosen property. Different ways are available to define the homogeneity of a region, which are based on objectives in the segmentation processes. It can be defined via the color, texture, gray level, layer depth, etc. Overlapping areas are not permitted, because each pixel belongs only to a single region. The aim is to let each region grow as large as possible under its certain characterization. This reduces the total number of regions (Navon et al., 2005). Many of the segmentation methods are based on two basic characteristics of the pixels in relation to their local neighborhood: discontinuity as well as similarity (Freixenet et al., 2002). The ideal segmentation of an image should result in a balance between over- and under segmentation of the file. The dominant method used for segmentation of remote sensing images is region-based segmentation, although it has some limitations. It is very time consuming to create a large number of heterogenous regions, starting with separate pixels (Gu et al., 2018). However, segmentation algorithms have advantages over pixel-based image classifiers. Final maps are typically more visually reliable and can be more effortlessly transferred into a GIS. Region-growing methods are mainly used for remote sensing tasks as they create closed regions (Tilton and Lawrence, 2000). Region-growing algorithms are mostly used for remote sensing images, as they guarantee creating closed regions. One of the challenges, when working with region-growing algorithms, is their need for user-supplied parameters to ensure best results as they depend strongly on these parameters (Espindola et al., 2006). The region-growing algorithm selects a set of seed points. This can be done either manually or automatically (Kamdi and Krishna, 2012). Current generations of region-growing algorithms are based on threshold values. Similarity and area threshold. It starts by checking neighboring pixels if they are similar and then merging them into regions. The results of the image segmentation are very susceptible through the user threshold value input. Values are between 0 and 1. Where 0 stands for excessive partitioning, resulting in confusing visual picture of the image.

1 forces the union of spectrally distinct regions, the result is undersegmentation (Espindola et al., 2006). The image segmentation in this thesis was done using i.segment in QGIS Processing toolbox. Tests showing the best threshold value to use for this purpose is 0.03. As illustrated
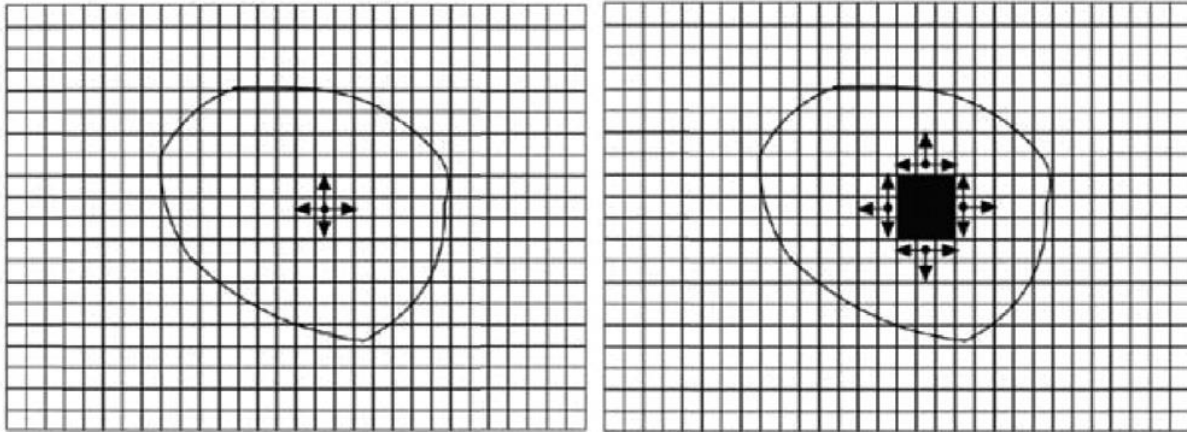
Figure 9: Region growing algorithm (Zhang et al., 2015)

in Figure 9 the algorithm sets seed points randomly. It keeps growing until it reaches a boundary. This boundary can be defined via the threshold value.

In general, it is easy to use as well as the robustness to noise (Zhang et al., 2015).

3.3. Zonal statistics

To develop and validate algorithms when using remote sensing images, statistics from individual pixels are mandatory. To reduce noise when working with classes or zones, it is eligible to take an average of a bigger number of pixels (Bunting et al., 2014). Zonal statistics can be extracted either from individual raster datasets or from two raster datasets. In most cases zonal statistics are computed using two raster datasets. In this case there is an input raster as well as a zonal raster. The input raster data sets typically contains thematic value information like type of land cover, temperature, elevation, slope, population etc.

Figure 10: Principle of operation
(http://desktop.arcgis.com/en/arcmap/10.3/tools/spatial-analyst-toolbox/GUID-407BA24C-A633-43A8-8D11-7A6FE3EF3609-web.png)

The zonal raster contains mostly regularized group of zones which consists of contiguous or noncontiguous zones of pixels. This can be information like individual counties in a state, districts, or arbitrary subdivisions such as rectangular tiles. Zonal statistics operation now creates a new output raster data set which summarizes the cell values in the input raster for each pixel in the zonal raster. The most common zonal statistics include minimum, maximum, mean, range, standard deviation values (Jensen and Jensen, 2013). Figure 10 showing working principal zonal statistic features. The aim is to eliminate mixed pixels (Saadat et al., 2011).

Zonal statistics for all images were acquired using Zonal statistics tool within the QGIS Processing Toolbox. As a result, for each file, there were 77 datasets available. These sets consists amongst other things minimum value, maximum value, sum, count of pixels, mean value, standard deviation, unique values, range values, variation, median, mode. These values were extracted for every single band, as well as for the NDVI (**N**ormalized **D**ifference **V**egetation **I**ndex) and NDWI (**N**ormalized **D**ifference **W**ater **I**ndex).

3.4.   Classification
3.4.1. Classification process
The spatial distribution of earth surface features is usually shown on a thematic map. Providing more an informational description rather than a data description. Image classification is the process which is used to produce thematic maps from satellite imagery (Schowengerdt, 1997). One of the main tasks in remote sensing applications is to classify the
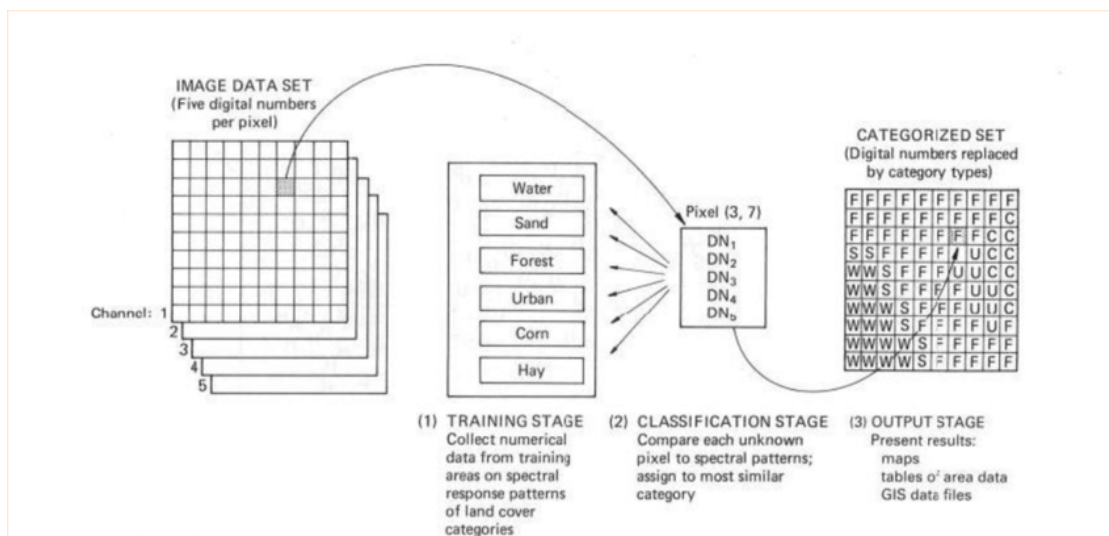
Figure 11:Data classification process (Alkhouri, 2014)

image pixels into homogenous areas, as these regions consist of different types of land covers

(Alok et al., 2016). This is usually done via two different approaches: per pixel and per object methods. Another important factor in image classification approach is the resolution of the input image (Bernardini et al., 2010). As mentioned by Gao and Mas (2008) traditional pixel based image classification is inadequate as it only uses spectral information of single pixels, which leads to poor results especially when using high resolution images. Due to the advanced sensors the field of spectral variability is increasing, which leads to lower accuracy using the traditional pixel-based approach. Figure 11 showing individual steps during the classification process.

3.4.2. Random forest classifier

To detect land cover changes in remote sensing images, a suitable classification method is required. The random forest classifier (RF) is a commanding machine learning algorithm which is the standardly used classifier in remote sensing by now. The RF can learn features of a target class from training data and is able to classify these learned characteristics in unclassified data (Belgiu and Drăguţ, 2016). The RF grows a lot of trees, where each tree is trained on a sample of the training data. Different classification approaches train numerous classifiers, combine their outcomes through a voting process. The most commonly used methods are boosting and bagging. Bagging is built on training numerous different classifiers on samples from the training dataset. This step reduces the variance of the classification. On the contrary, boosting uses iterative re-training. Here the inaccurately classified examples are given more weight in each consecutive repetition. On the one hand, this makes the algorithm slow, on the other hand it is usually more accurate than bagging (Gislason et al., 2004). The machine learning algorithm is an automated supervised classification as it predicts the object types by using the characteristics from the input training data(Dubath et al., 2011). The RF consists of a mixture of tree classifiers, where each classifier is created using a random vector which is sampled independently from the input data. Each individual tree casts a vote for each class to classify an input vector (Pal, 2005). As the tree is created from training examples, it may be afflicted from overfitting when the complete structure is reached. This might worsen the accuracy of the classification when the tree is working on unseen data and therefore this can lead to less generalization ability (Xu et al., 2005). Significant improvements have led to an increasing classification accuracy (Breiman, 2001). A major advantage of the random forest classifier is shown by Gislason et al. (2006). In this paper they demonstrate that the RF does not overfit, and that the algorithm can also estimate the importance of variables for the classification

process. It also does not tend to over-adjustment if more decision trees are added (Rodriguez-Galiano et al., 2012). The random forest classifier is strong against outliers within the training data set as well. It also produces respectable results when using noisy data (Zhang et al., 2017). As shown by Belgiu and Drăguţ (2016) the precision of the random forest classifier is decreasing when the algorithm is trained on diverse study areas. Tests also showing, that the classification model is not transferable to other zones.

3.4.3. Training data

The selection of training data as well as detailed input variables, having a large influence on the general precision of the image classification. The results are susceptible to the size of the training data set. Training data should be as large as possible, as well randomly spread to be representative of the actual class scopes in the scenery. Furthermore, they ought to have negligible spatial autocorrelation to enhance classification results (Millard and Richardson, 2015). Training data in image classification tends to completely label every class spectrally, therefore a huge number of samples is required. However it is sometimes possible to select the most useful training samples, allowing you get accurate classification results from smaller training samples (Foody and Mathur, 2004).

The procedure in this thesis was to identify appropriate training areas in each study site. Requirements were versatile as the data had to include each landscape typology which should be classified later. The data set must also be within the right size, as there should be enough data for the classifier to learn and identify the classes on its own. Furthermore, more suitable data had to be available to validate the trained classes on new data. Thirty percent of the training data was used to train the classifier, the remaining seventy percent were used for subsequent validation. Only when this validation was successful, the script using all the available data was started.

3.5.   Software and processing environment

The classification process within this thesis is based on a Python script, using Jupyter notebook.

Traditionally, scientific computing focused either on raw performance (e.g. C/C++) or systems like Mathematica or Matlab. Python provides access which goes beyond to solve just pure numerics. Python was planned to use a general-purpose language. It is an object-oriented language which lets users redefine the sense of most operators (Perez et al., 2010). A clear syntax makes the code easy to understand and read. These codes are separated into logical clusters. Such as modules, classes and functions (Oliphant, 2007). Scikit-learn is a Python module which integrates a widespread variety of different machine learning algorithms for supervised and unsupervised difficulties. The main advantage of Scikit-learn is that it's simple for non-specialists to use. It provides modern implementations for many different machine learning algorithms. The user interface is easy to use (Pedregosa et al., 2011). In general, notebooks are intended to assist the workflow of scientific computing. The code in a Jupyter notebook is arranged in cells, which can be separately modified and run. The cell output is appearing straight underneath the cell and is stored as a part of the file. The direct output of each cell can include not just text, but also plots, mathematical equations or graphics. It is also possible to highlight individual parts. Jupyter is an open source development, which can work with diverse programming languages. More than 50 different codes have been tested successfully using Jupyter notebook so far. The access to Jupyter Notebook is via a modern web browser. That's the only software required. The resulting files are documented JSON format with an '.ipynb' ending. It is also easy to share the notebook with other users (Kluyver et al., 2016). Jupyter Notebook is intended as set-up for reproducible different workflows. The main intention is to maintain a record of workflow implementation (Yin et al., 2017). Most commonly used is the Python language which is also an open source product with a huge variety of work packages for data experts, allowing you amongst others to process, analyze and visualize data (De Marchi et al., 2017). The possibilities Jupyter notebook offers are shown by Leonard et al. (2019), where they develop a participatory Green Infrastructure (GI) design. This is mostly used by land use planners, landscape architects as well as water resource managers. This is to endorse ecosystem services like alleviation of storm water flooding and water quality deterioration.

4. Results

The results relate to the respective study areas and are presented both technically and scientifically.

4.1. Drew Point

At Drew Point in Alaska, ongoing costal erosion was detected.

Figure 12 showing Drew Point after the image segmentation. It was recorded on the 28th of June 2017. The coast line is clearly visible, as well as the sheets of floating ice.
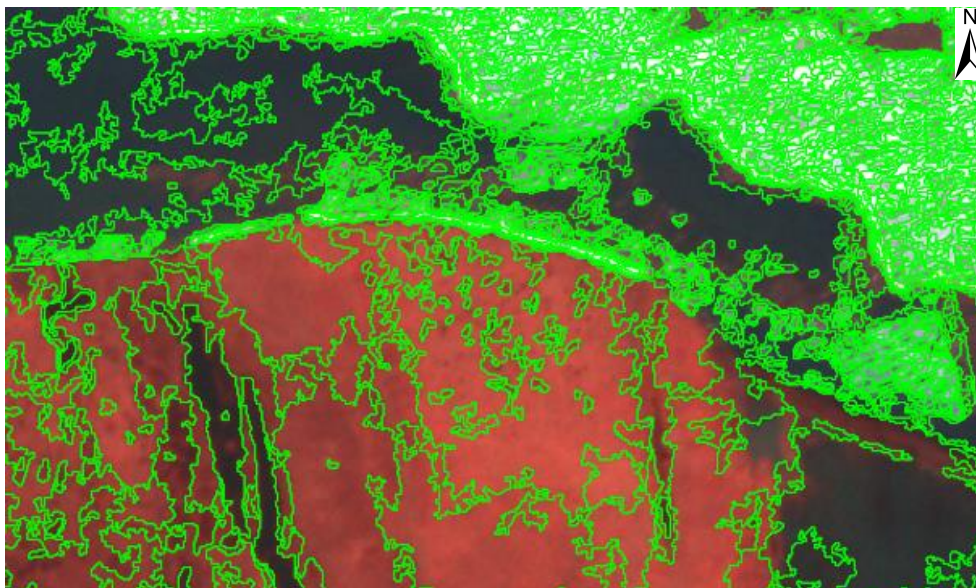
Figure 12: Image segmentation Drew Point, AK

The training area was chosen quite at a small-scale. Since it includes all necessary classes, the size is appropriate. It is illustrated in Figure 13 below.
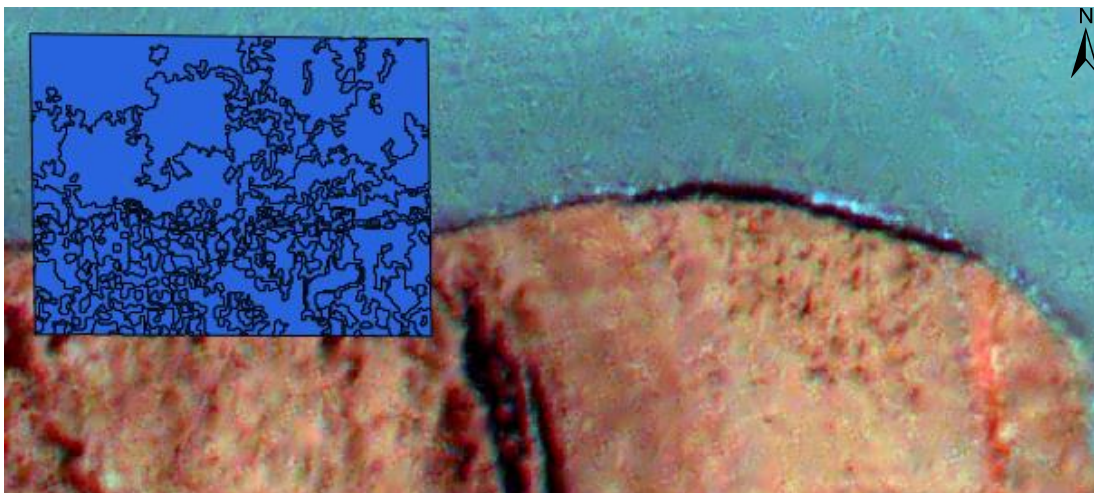
Figure 13: Training area Drew Point, AK

Classification results showing that more than 185.000 polygons out of roughly 1.6million were detected with a probability greater than 69%. This number indicates the likelihood that this polygon is water. It should be noted, that the number of polygons does not consider the size of the polygon.

Figure 14 showing the advancing coastal erosion in the year 2017. The outlines have been traced manually. The green line in showing the position of the coast on the 28th of June 2017, blue line indicating 28th of July and the yellow line at the end of September. The biggest difference between these lines showing a rate of erosion of about 35 meters.

Figure 15 below exhibit the situation at the same spot in 2018. As in 2017 coastal erosion continued, but a little bit less extensive. Maximum rate of erosion is 21 meters. The total erosion between June 2017 and October 2018 at this point was at about 56m.
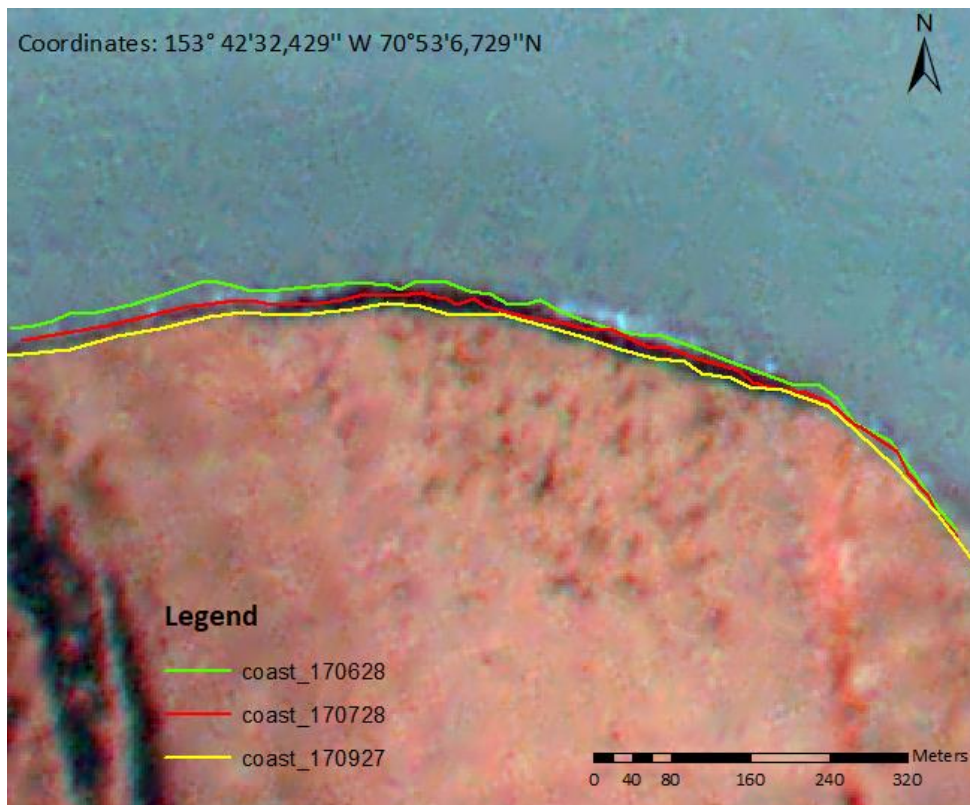
Figure 14: Resulting coastal erosion Drew Point, AK, 2017 – Image: 2017_09_27.tiff
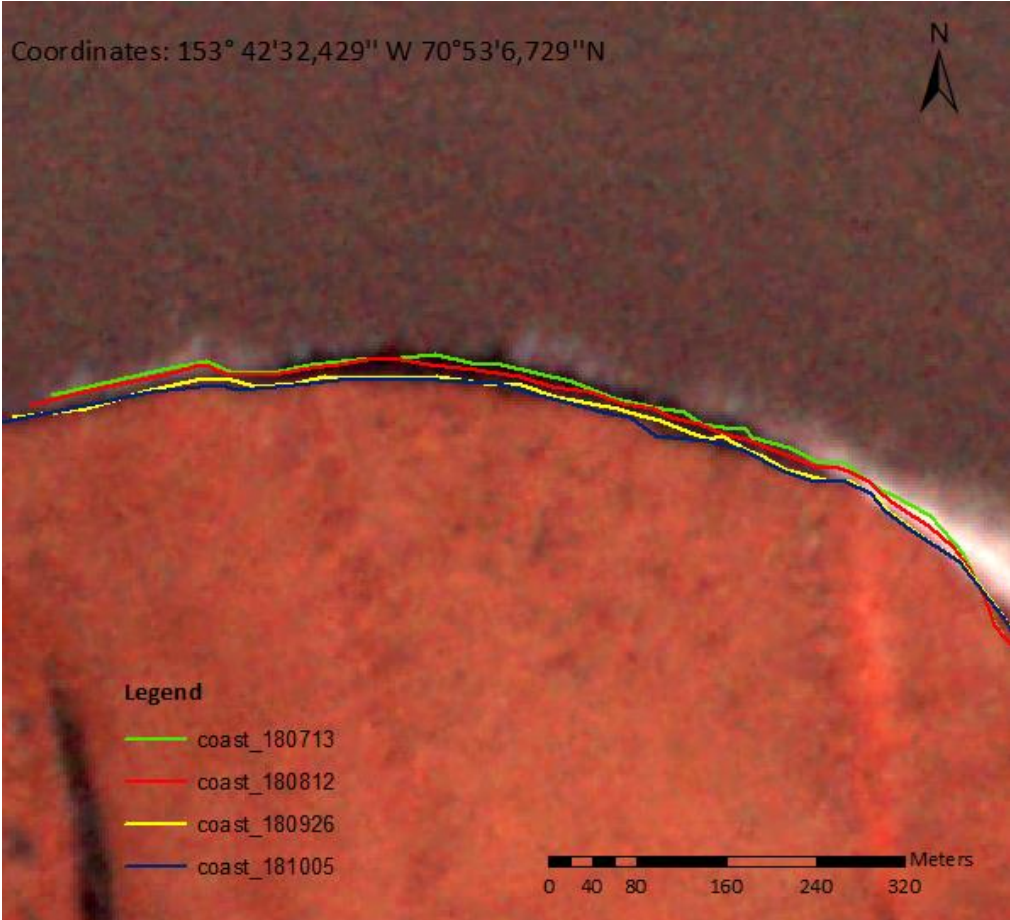
Figure 15: Resulting coastal erosion Drew Point, AK, 2018 – Image: 1747381_0571814_2018-10-05_0f35_BGRN_Analytic.tif

Technically good results could be achieved. As an example, see Image 16 below. However, the coastal outlines could not be traced fully automatically as the results would lead to inaccurate outcomes. A deeper insight in to the reasons can be found in the discussion chapter.
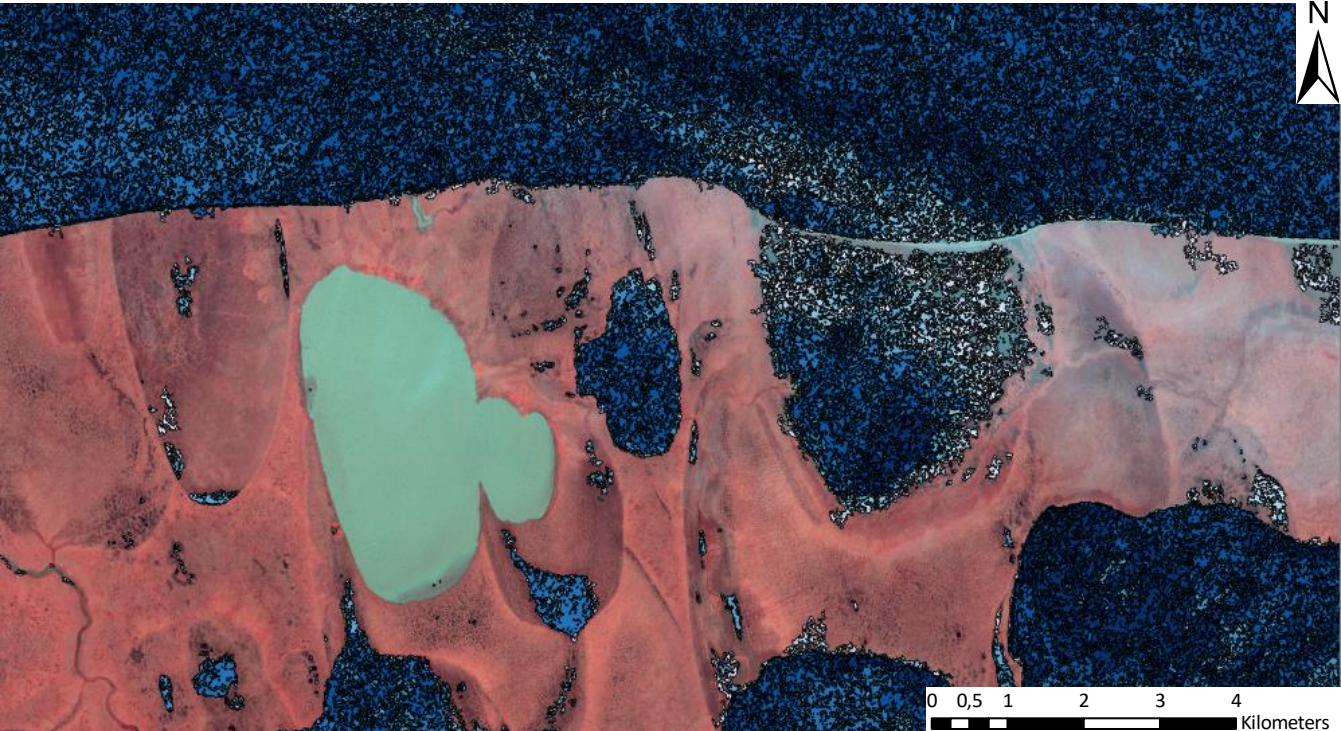
Figure 16: Image segments classified as water Drew Point, AK

4.2. Noatak Valley

In Noatak Valley, retrogressive thaw slumps have been detected. Due to technical reasons, the slump outlines have been traced manually to show a better view of the sub-annual changes.
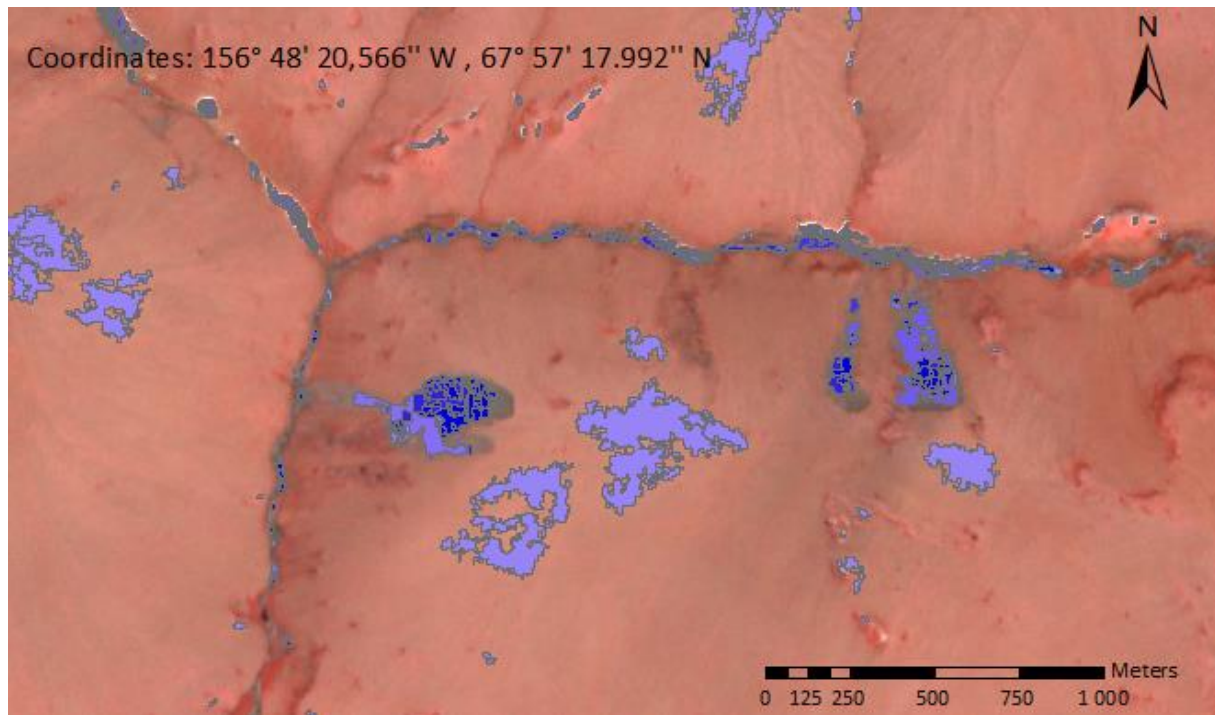
Figure 17: Results automatic classification thaw slumps, Noatak Valley

Unfortunately, it was not always possible to separate the slumps clearly from the surrounding landscape during the automatic detection (See Figure 17). The reasons for this are manifold and are explained in the technical review. To compare the landscape changes, the outlines of the thaw slumps were detected manually.

In Figure 18 the biggest detected slumps in Noatak Valley including their changes are shown. The upper image displays the changes in the period June to September 2017. In every area a headwall retreat of roughly 25 meters could be measured. The image below showing landscape changes between June and October 2018. The slump on left hand side increased up to 40 meters uphill. The slump in the middle of the image shifted 28 meters uphill, whereas the right slump shifted by 35 meters.
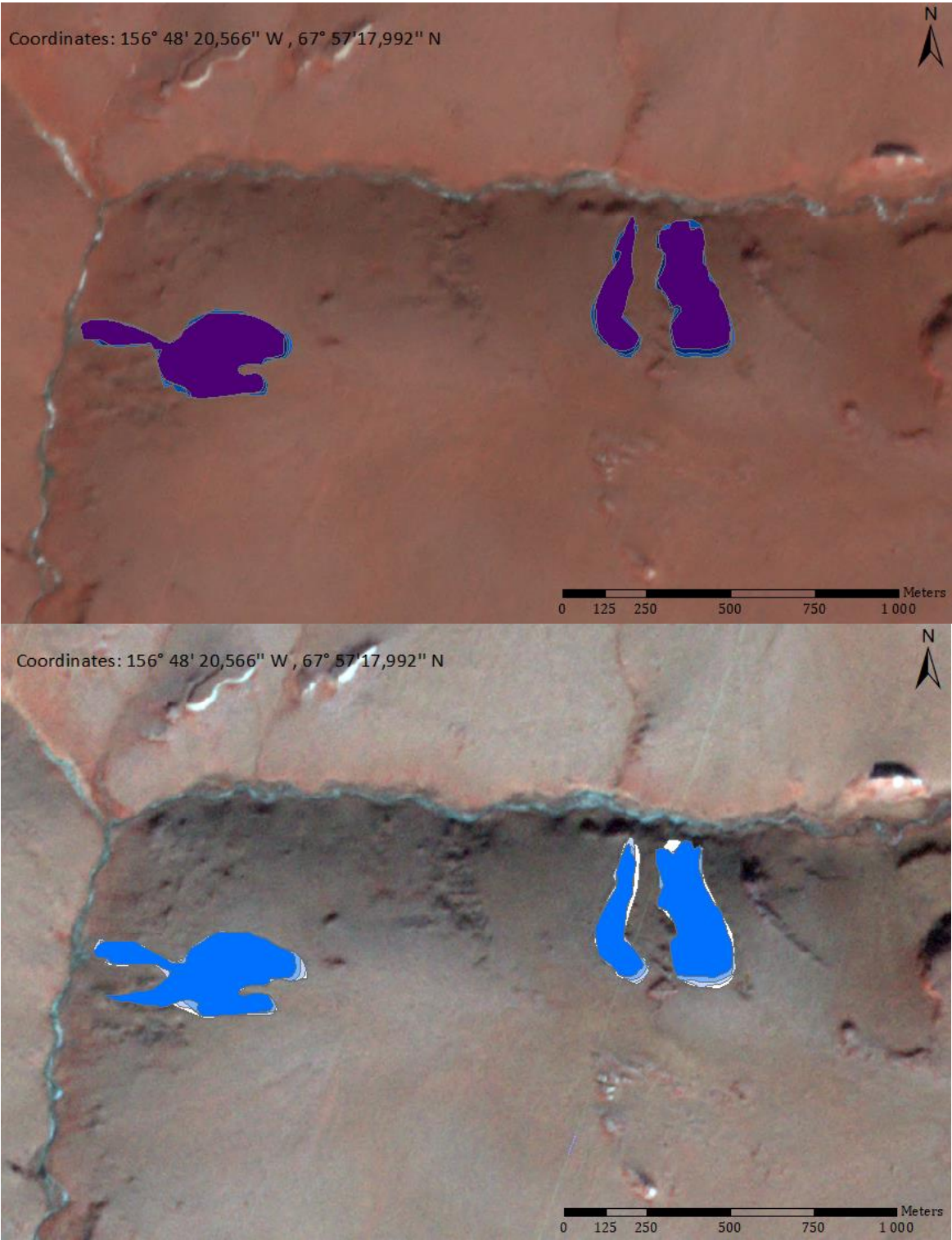
Figure 18: Comparison thaw slumps 2017 - 2018

The total changes between June 2017 and October 2018 are displayed in Figure 19 below.
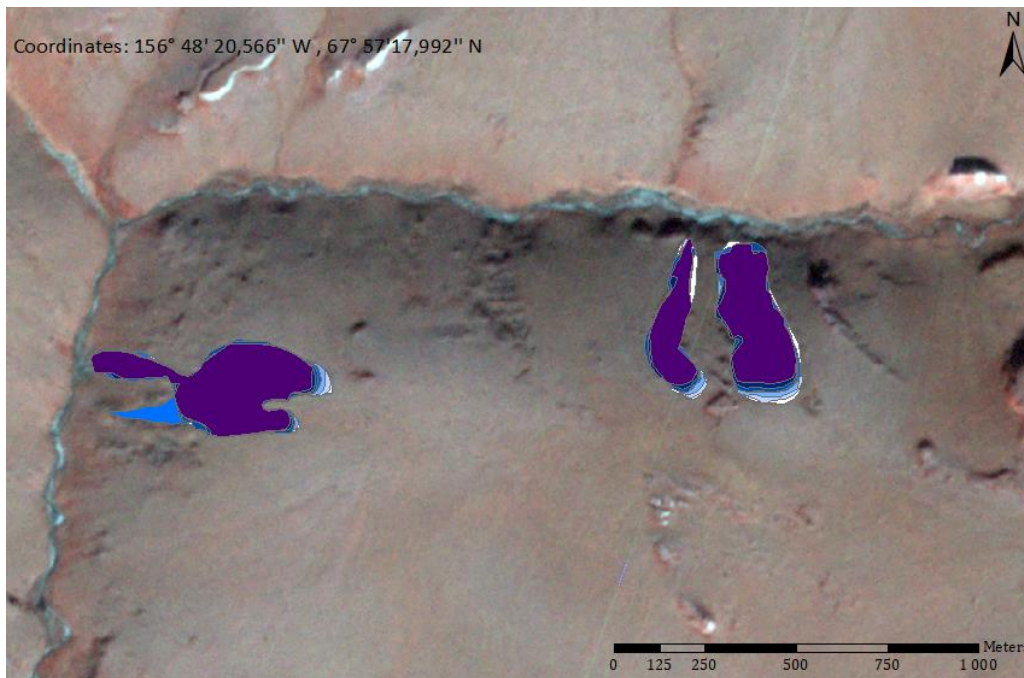
Figure 19: Total changes thaw slumps

From the technical point of view, the automatic detection turned out to be difficult. One of the better results can be seen in Image 20. For further details and explanations see discussion chapter (5.1.).
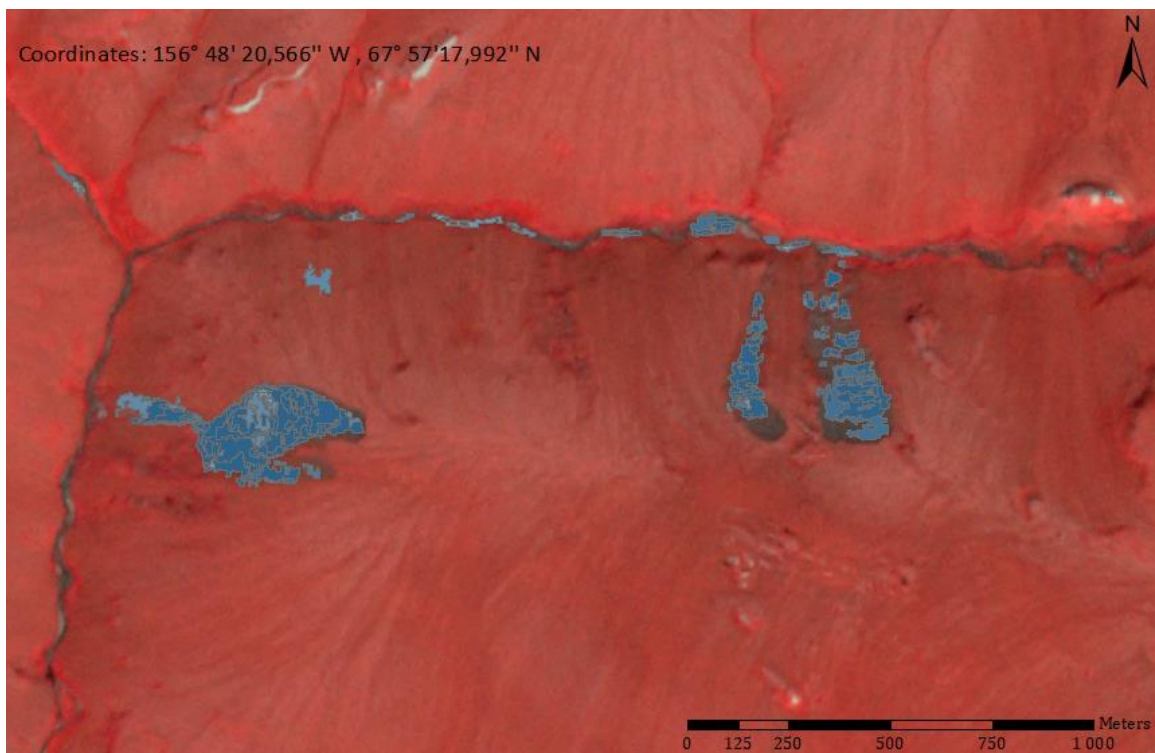
Figure 20: Automatic classification retrogressive thaw slump, Noatak Valley

Beside the automatic detection, the results have also been compared with a Landsat dataset from the time period 1999 – 2014. In the image below (Figure 21) the Landsat results are dyed green. In general most of the active slumps in Noatak Valley could be detected although the image resolution is 30m, compared to 3m Planet reolution. But as Figure 22 shows on the left hand image, a thawslump was detected, although there is none.
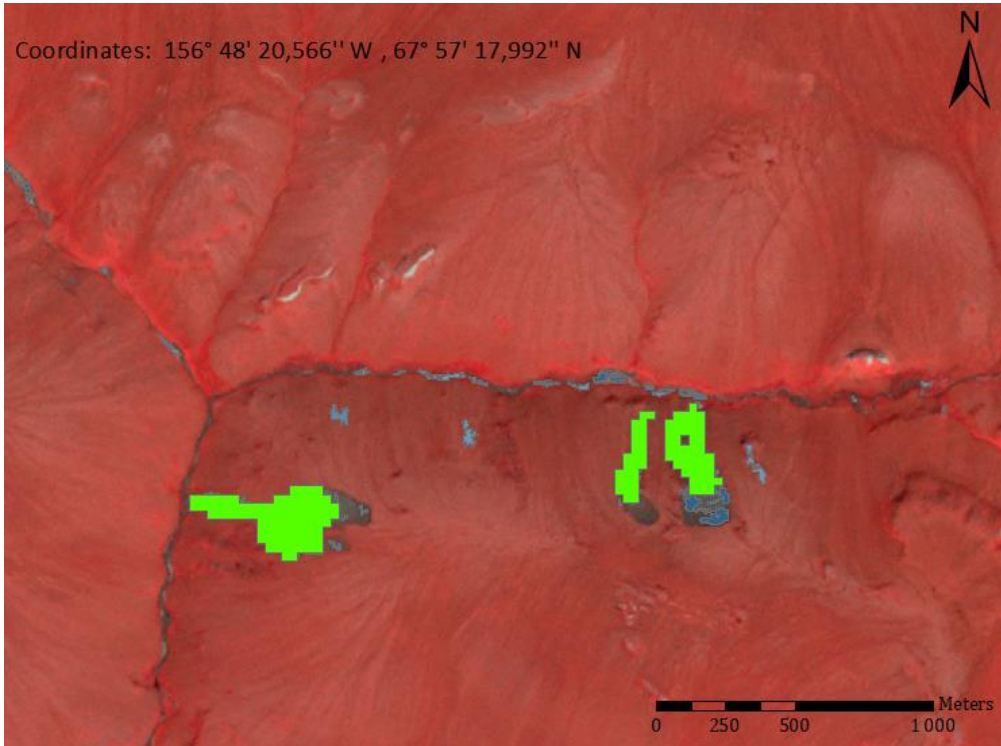
Figure 21: Landsat vs. Planet data, Noatak Valley
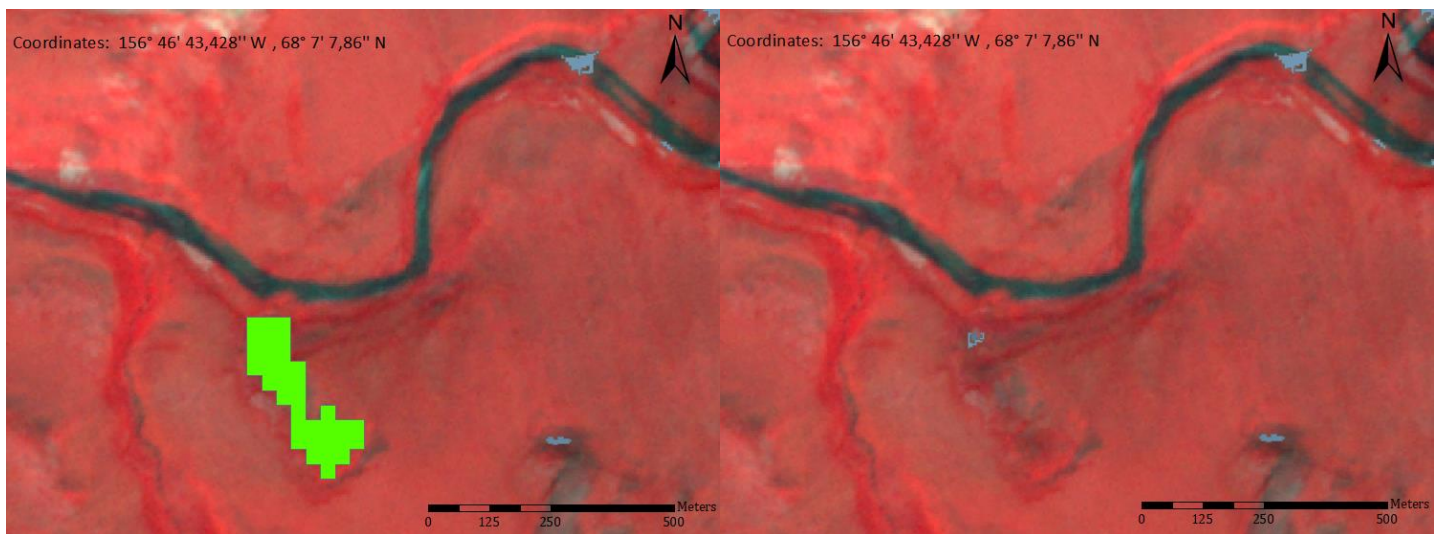
Figure 22: Landsat detection, Noatak Valley

4.3. Central Yakutia

In the Yakutia area, lake changes were detected. Each color indicating a recording date. Due to the size of the image section of about 400 square kilometers only details are shown. As seen in the image below (Figure 24) the lakes in the area tend to be very stable throughout the year, no huge changes could be detected. The same result could be observed in 2018, which is visible in Figure 25.
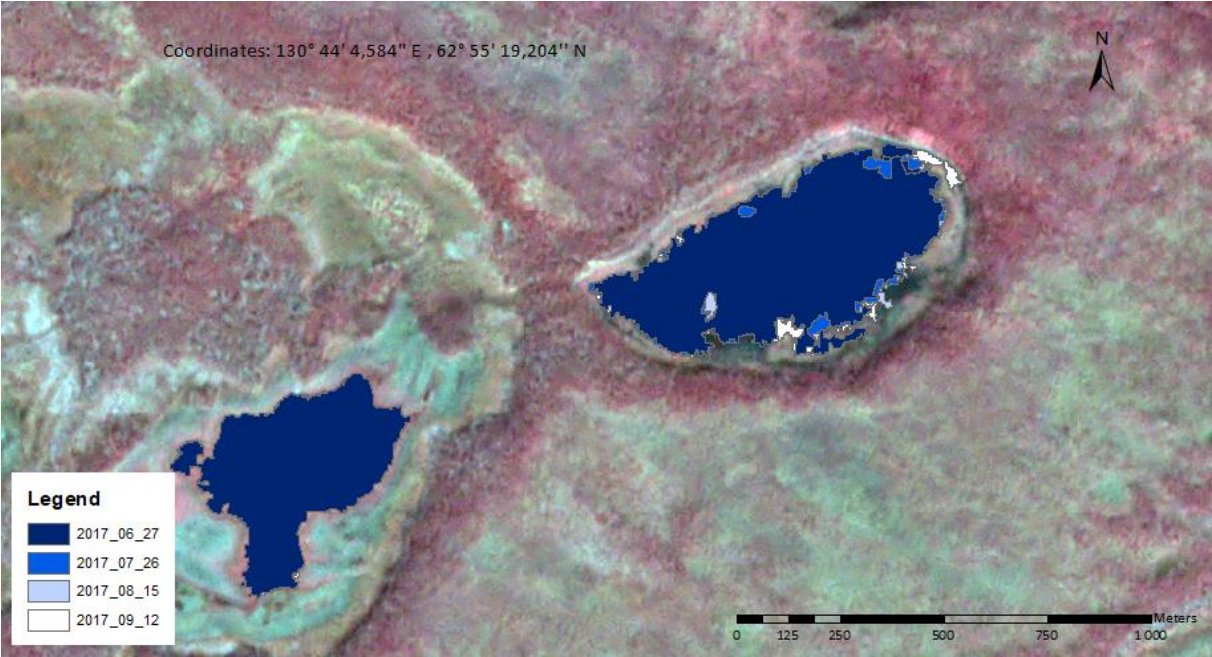
Figure 24: Lake Central Yakutia, 2017
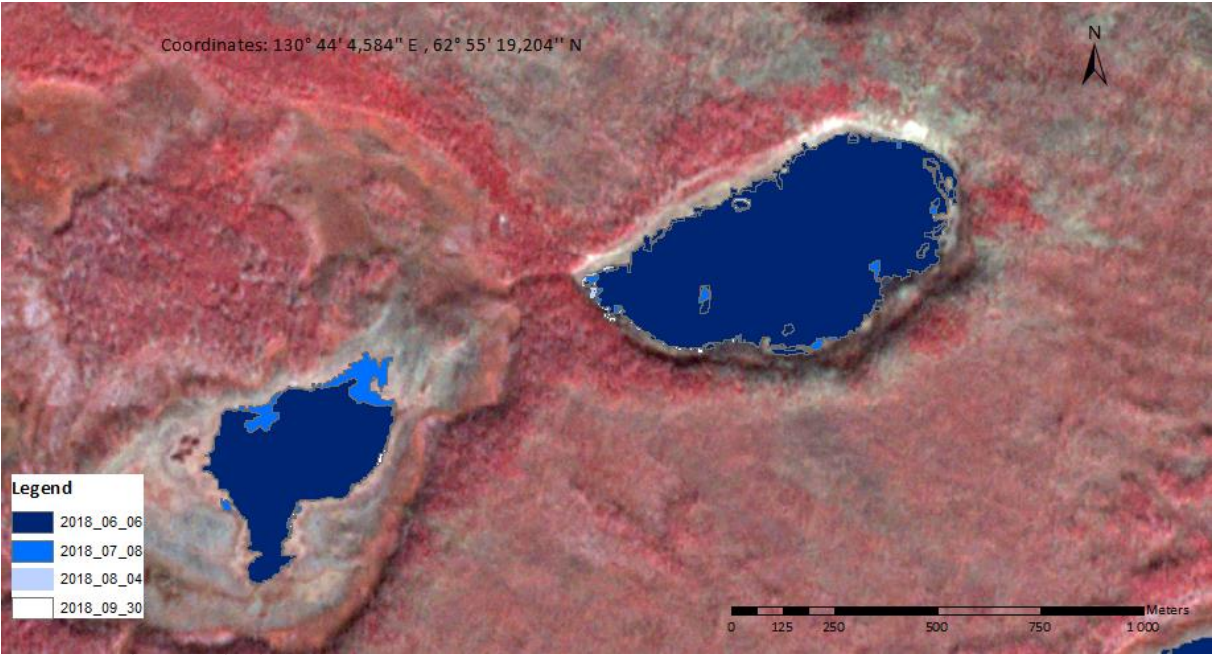
Figure 25: Lake Central Yakutia, 2018

Technically the results are displayed in Image 26, each of the detected lakes was hatched.

Each cross hatch respectively color symbolizing a date. It turns out that most of the lakes

were well detected. The lakes on the left side are not displayed because only the

overlapping area was selected.
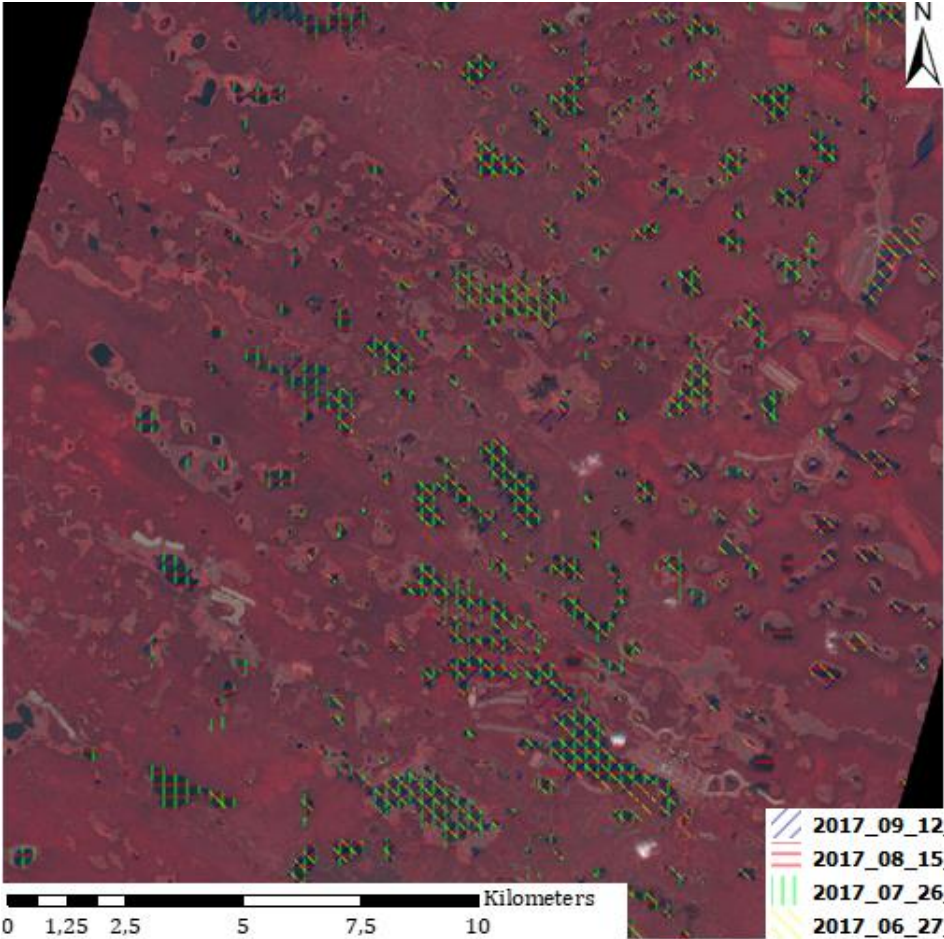
Figure 26: Detected lakes Central Yakutia

5. Discussion

This thesis was considered to investigate the possibility of an automatic detection of landscape changes in permafrost areas using Planet Cube Sat data. The focus was set both on a technical as well as a natural scientific point of view. The already known methods as well as some new ones revealed a highly changing landscape in Alaska, and a more static in Siberia. The following discussion is split in two parts, a technical review followed by a scientific evaluation.

5.1. Technical discussion

From the technical point of view several difficulties within the different methods have occurred.

Data acquisition:

The data acquisition using the Planet API downloader was simple and effective. The required data could be downloaded after adapting the tutorial for the personal needs. It is necessary to be careful which type of data you acquire, as there are different possibilities which include the Basic scene, Ortho scenes as well as Ortho tile scene (for further information see 1.1.2). After the data type selection is done, you receive a download link which is valid for 5 minutes. By clicking on it, the download starts, and you can save the image to your device.

Image segmentation and region growing algorithm:

The image segmentation and the region growing algorithm partly showed some weaknesses. As shown in Figure 27 on the left-hand side, the edge of the retrogressive thaw slump could not be clearly differentiated from the surrounding landscape. This leads to the emergence of a large polygon which includes part of the thaw slump as well as a part of the landscape. The same problem could be observed at Drew Point. When looking at the right side of Figure 27, you'll notice that the resulting polygon consists of water and land. In this case it can be assumed that the darker color in the landscape as well as the dark color at the cliff is responsible for the accruement of that specific polygon. In a further consequence, the automatic detection produces impure results. Of course, there are more reasons for getting bad results. But if there is a clear difference in color value, as shown in Figure 28, the algorithm delivers good outcomes. The differences of the chromaticity are big enough to achieve a clear demarcation. With other software, the form could also be entered as a criterion.
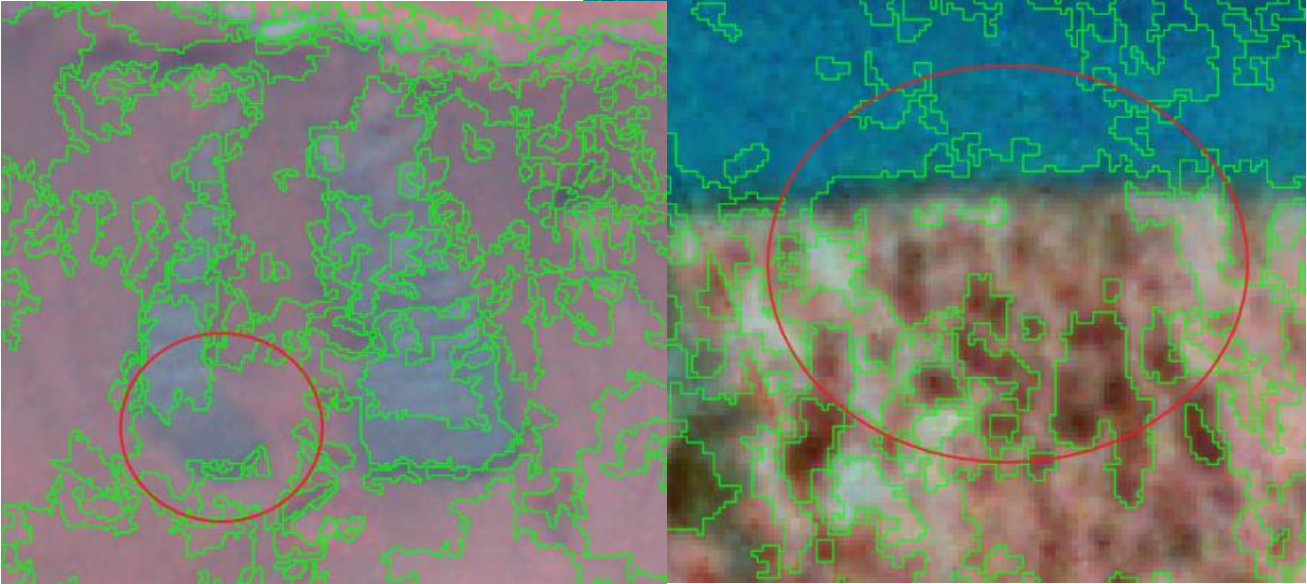
Figure 27: Thaw slump image segmentation left; Drew Point image segmentation right
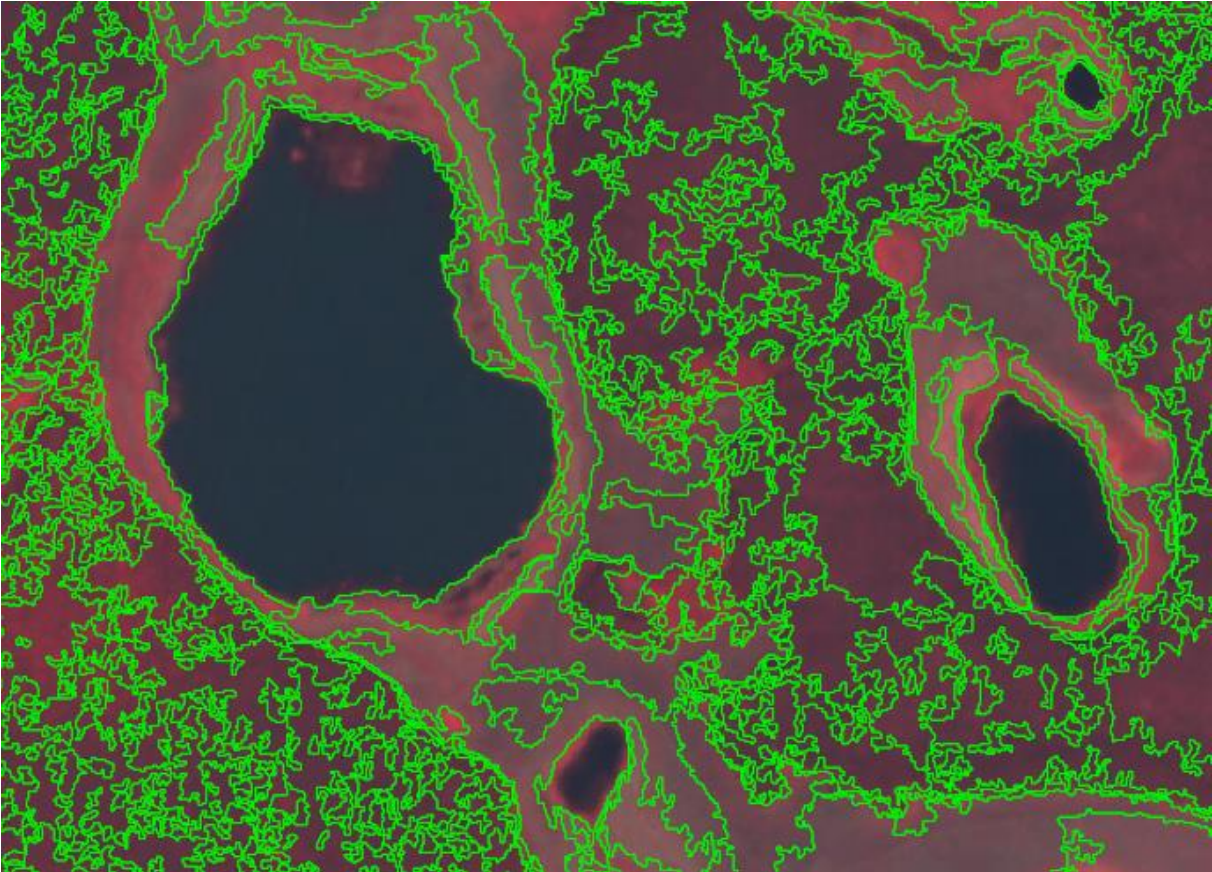
Figure 28: Image segmentation, Siberia

Zonal statistics:

Overfitting is a well-known problem in machine learning. The best way is frugality, the model needs all the necessary input data, but nothing more (Hawkins, 2004). If the algorithm uses many unnecessary features this can lead to overfitting in training and therefore low precision in testing. In this context, the algorithm memorizes non-predictive structures of the training data instead of learning to simplify from a tendency (Xiaoyue et al., 2017). Another reason for overfitting can be random noise, at the signal to noise ratio (M. Sousa and Åberg, 2018). When using Jupyter Notebook, it has been determined that too much data may be available. It can be assumed that the large number leads to overfitting.

It cannot be clearly determined if more or less zonal statistic data would have led to better results. During initial test phase, no differences were observed when using all 77 features or just the top 20 features regarding their importance. So, the direct influence of the zonal statistic remains unclear at that point. It is assumed that the enormous amount of data may also led to overfitting as the results may correspond too closely to the training data set.

Training data:

As mentioned by Foody et al. (2006) the selection of training data for a supervised classification in remote sensing, should encompass all the features. The size of the training area can be small if it ensures an appropriate classification. Especially if you are interested in just a single class.

The used training data for all different study sites were chosen randomly. The only condition was that all the different landscape forms needed to be within the training data, otherwise a classification would not be successful. The different training data sets from Siberia and Drew Point didn't really have a huge impact on the outcome of the final classification. Several sets were tested. In contrast in Noatak Valley differences in the results could be observed. It is assumed that the variation of spectral values within the whole study area (roughly 800km²) is a factor for the further classification and the automatic detection.

Random forest classifier

When it comes to remote sensing and image processing the random forest classifier is the standard algorithm used. It received more and more adherence over the last decade as it led to stunning classification results in combination with an astonishing processing speed

(Du et al., 2015). The random forest classifier uses about two third of its input data for training the trees while validating the results using the other third of the data and check how well the resulting random forest classifier model executes (Belgiu and Drăguţ, 2016). Interestingly the number of trees doesn't have an impact on the output of the data as tested by Du et al. (2015) They tested the sensitivity of the random forest classifier from 10 to 200 trees and didn't notice any difference in their results. In general, random forest classifier is less prone to overfitting than other machine learning classifiers, because of its large number of decision trees (Belgiu and Drăguţ, 2016).

All these mentioned statements above can be confirmed, as the same experiences during the emergence of this thesis were made. Different numbers of decision trees were tested during the data classification phase, but the outcome was still the same. All in all, the random forest classifier is a decent possibility to get good and meaningful results. Although the final results were not always as desired, the machine learning algorithm cannot be held responsible.

Software processing and environment:

The self-written Python script was based on a script developed during the internship in Potsdam. For lake detection and coastal erosion only, a few changes were required. When it comes to retrogressive thaw slumps the script needed a whole revision. A single script was written for training and a second one for the classification and validation. To achieve better results different input images have been tested. Unfortunately, the results didn't vary too much.

Classification:

The classification results varied strongly not just study site to study site but also within a study site as different dates showed different results. Especially in Noatak Valley the different input images led to varying results, although nothing was changed within the Python script. It can be assumed that the multispectral values scattered too much. As a result, the values are outside the threshold for the thaw slump class and were therefore classified incorrectly. The classification in Siberia as well at Drew Point showed fewer problems. Not all the features could be clearly identified, but the results show that the script works in general.

Further notes:

In the final part of this technical review a few more points should be briefly addressed.

- Software: The used software was mainly QGIS. As it is an open source product which is regularly improved by users, it is a very valuable software. Although maybe other software would have led to better results. Especially eCognition should be mentioned here. The biggest disadvantage when using eCognition is the high price for a license.

- Tests during the initial phase also showed that upsampling is better than downsampling. Usually upsampled images lack of small scale texture-related features (Fattal, 2007). In this case the proportion of landscape polygons vs. thaw slumps polygons was very diverse. In Noatak Valley were roughly 400.000 landscape polygons and a little bit more than 2.000 thaw slump polygons. To make the detection more sufficient, this step needed to be taken.

- Planet satellite data options are limited due to the four different bands (RGB + NIR). It is assumed that more bands would further improve the accuracy of the results. Nevertheless, Planet offers an amazing product. Due to its low weight, the lack of jet propulsion, as well as the large number of microsatellites, Planet manages to provide the end user a large amount of data at a reasonable price (if more than 10.000km² per month are required).

5.2.   Scientific discussion

5.2.1. Drew Point, Alaska

Coastal erosion at Drew Point varied from 35m yr^{-1} in 2017 to 21m yr^{-1} in 2018. A reason for these different numbers could not be clarified as there are many different variables. There is no clear tendency to see if the erosion is stronger in the beginning or the end of the ice-free season of the Beaufort Sea. This could be either due to severe weather events or other factors which are not known yet. Most likely a long sea-ice season was responsible, by looking at the satellite images, in 2017 the Beaufort Sea was ice-free by the end of June. 2018 the ice-free season ended about one month later. Another possible reason for the high rates of erosion can be explained when looking a Figure 29.
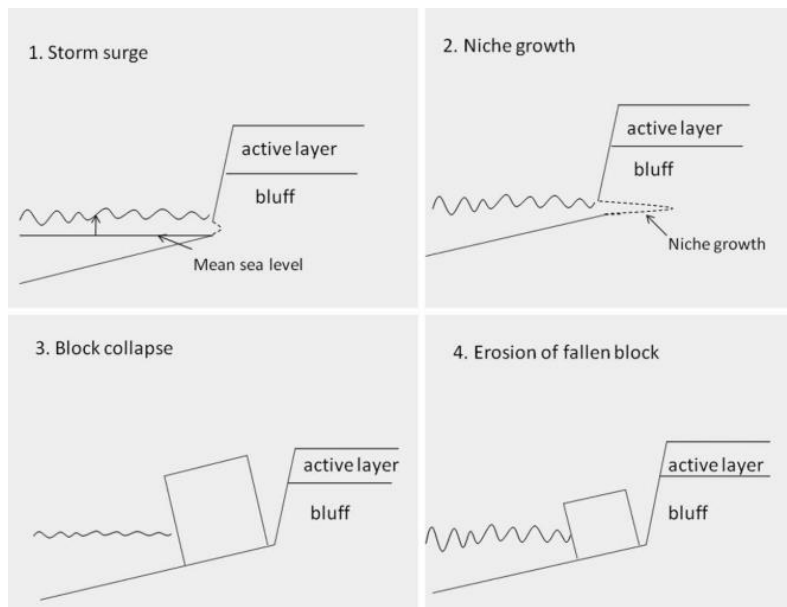
If there is a storm event, the rising water leads to contact between the sea and the permafrost bluff. Because of the permanent and strong movement of the water a niche is growing. A block above the niche is collapsing and is eroded into the Beaufort Sea (Ravens et al., 2012).

Figure 29: Model of block collapse (Ravens et al., 2012)

The detected results correlate with the number from Jones et al. (2018a) in their paper where the observed mean coastal erosion at Drew Point varied from 6m yr^{-1} to 23m yr^{-1} with a maximum erosion of 48.8 meters. The second study by Jones et al. (2018b) revealed also similar numbers at Drew Point.

5.2.2. Noatak Valley

In Noatak Valley the detected retrogressive thaw slumps shifted 25 to 40 m yr^{-1} uphill. That's about the same numbers that Swanson and Nolan (2018) mention in their study in Noatak Valley. They measured maximum growth rate of 38 m yr^{-1}. Due to their in-situ measurements and their airborne GPS camera, they were able to detect elevation changes of 10 to 15cm. It is assumed that the slump growth rates are going to decrease as soon as they reach a more gentle topography. The thaw season usually extends from mid-May to mid-September (Panda et al., 2016). Height of the scarp and growth-rate of the thaw slump are closely related to slump ground ice characteristics. Slumps with an exposed ice-wedge tend to have higher scarp heights than slumps without an ice-wedge (Swanson and Nolan, 2018). Compared to these numbers, the growth rates of retrogressive thaw slumps in Siberia is marginal. The average headwall retreat in Central Yakutia is between 0.5m and 3.16m yr^{-1} (Séjourné et al., 2015). The exact reasons for the different rates cannot be determined yet. In Central Yakutia, however, less research has been done.

5.2.3. Central Yakutia

In Siberia no major changes of thermokarst lakes could be detected. Thermokarst lakes in regions with large and deep ice-wedges (like Yakutia region) depths usually don't exceed 25meters. Deep lakes usually don't tend to drain. As mentioned by Smith et al. (2005) the regional setting in Siberia is responsible for lake expansion or lake decline. In areas with continuous permafrost, lakes tend to be stable or to increase. From 1973 – 1998 the lake area in Siberia raised about 12 percent. In discontinuous, sporadic or isolated areas the lake size declined about 12 percent. As shown by Schneider and Hook (2010) due to the ongoing climate change lakes are warming quickly. This impacts not only thermokarst lakes itself, it would also have consequences for the morphological as well as hydrological dynamics.

As Central Yakutia lies within a zone of continuous permafrost it is plausible that only small areal changes could be detected at the thermokarst lakes. Perhaps the changes have been too small to detect, or it has been two years where the climate has generally not contributed to a change in lake size.

6. Conclusion

The aim of this research was to detect and analyze different landscape processes in thermokarst areas automatically and to answer the following research questions:

- Do highly spatial and temporal resolved Planet cube-sat data have the potential to detect and quantify thermokarst related landscape dynamics?

  Yes, a 3-meter image resolution is adequate to detect the desired processes. As the comparison with lower-resolution data shows, it can also be used to detect different landscape processes.

- Can the occurrence and sub-annual temporal and spatial patterns of these detected thermokarst features be analyzed by a machine-learning algorithm?

  Yes, no and yes. It depends on the process you are looking at. The coastal erosion in Alaska could be detected very well and delivered good results. Unfortunately, the retrogressive thaw slumps in Noatak Valley could not be exactly detected. Different problems within the methodology occurred. Thermokarst lakes in Siberia however, could be detected clearly. Regrettably no lake drainage could be observed in that area.

- How do the Planet cube-sat derived thermokarst feature datasets compare to existing data products based on lower-resolution Landsat data?

  Surprisingly there was no big difference in detection when using Landsat or Planet data. The available Landsat dataset indicated the same areas, but a bit more inaccurate, compared to the best Planet results in Noatak Valley.

Especially the problems with the detection of the retrogressive thaw slumps put me in front of a task that could not be solved so far. As a result, one could try to use other software or other satellite images with more bands, this would perhaps lead to better results. Another way to achieve better results would be additional help from an expert in machine learning.

Future outlook:

From the technical point of view, I expect better results in the future. On the one hand because of better software environment and available data on the other hand as there are still a lot of different processes which are not fairly understood and need to be further explored. Planet plans to deploy satellites into orbit with six bands. This will certainly further increase the accuracy of an automatic detection.

From a scientific point of view, I hope that these processes can be stopped to some degree, as they point to climate change. Conversely, this would also mean that climate change was partially contained. Especially for ecosystems, residents as well as infrastructure in the affected regions, this would lead to positive effects.

7. Bibliography

ALEKSYUTINA, D., NOVIKOVA, A., BARANSKAYA, A., SHILOVA, O. & OGORODOV, S. 2018. USING MULTI-TEMPORAL AERIAL AND SPACE IMAGERY FOR COASTAL DYNAMICS INVESTIGATIONS AT KARA AND PECHORA SEAS, RUSSIAN ARCTIC. *Proceedings of the International Multidisciplinary Scientific GeoConference SGEM,* 18**,** 265-272.

ALESSA, L., KLISKEY, A., LAMMERS, R., ARP, C., WHITE, D., HINZMAN, L. & BUSEY, R. 2008. The Arctic Water Resource Vulnerability Index: An Integrated Assessment Tool for Community Resilience and Vulnerability with Respect to Freshwater. *Environmental Management,* 42**,** 523-541.

ALOK, A. K., SAHA, S. & EKBAL, A. 2016. Multi-objective semi-supervised clustering for automatic pixel classification from remote sensing imagery. *Soft Computing,* 20**,** 4733-4751.

ARÉ, F. E. 1988. Thermal abrasion of sea coasts (part I) *Polar Geography and Geology,* 12**,** 1-157.

ARP, C. D., JONES, B. M., SCHMUTZ, J. A., URBAN, F. E. & JORGENSON, M. T. 2010. Two mechanisms of aquatic and terrestrial habitat change along an Alaskan Arctic coastline. *Polar Biology,* 33**,** 1629-1640.

BARNHART, K. R., ANDERSON, R. S., OVEREEM, I., WOBUS, C., CLOW, G. D. & URBAN, F. E. 2014. Modeling erosion of ice-rich permafrost bluffs along the Alaskan Beaufort Sea coast. *Journal of Geophysical Research: Earth Surface,* 119**,** 1155-1179.

BELGIU, M. & DRĂGUŢ, L. 2016. Random forest in remote sensing: A review of applications and future directions. *ISPRS Journal of Photogrammetry and Remote Sensing,* 114**,** 24-31.

BELOVA, N. 2018. GROUND ICE AND ITS' INFLUENCE ON COASTAL EROSION OF KARA SEA REGION, RUSSIAN ARCTIC. *Proceedings of the International Multidisciplinary Scientific GeoConference SGEM,* 18**,** 173-179.

BERNARDINI, A., FRONTONI, E., MALINVERNI, E. S., MANCINI, A., TASSETTI, A. N. & ZINGARETTI, P. 2010. Pixel, object and hybrid classification comparisons. *Journal of Spatial Science,* 55**,** 43-54.

BETTS, E. D. & KANE, D. L. 2014. Linking North Slope of Alaska climate, hydrology, and fish migration. *Hydrology Research,* 46**,** 578-590.

BISKABORN, B. K., SMITH, S. L., NOETZLI, J., MATTHES, H., VIEIRA, G., STRELETSKIY, D. A., SCHOENEICH, P., ROMANOVSKY, V. E., LEWKOWICZ, A. G., ABRAMOV, A., ALLARD, M., BOIKE, J., CABLE, W. L., CHRISTIANSEN, H. H., DELALOYE, R., DIEKMANN, B., DROZDOV, D., ETZELMÜLLER, B., GROSSE, G., GUGLIELMIN, M., INGEMAN-NIELSEN, T., ISAKSEN, K., ISHIKAWA, M., JOHANSSON, M., JOHANNSSON, H., JOO, A., KAVERIN, D., KHOLODOV, A., KONSTANTINOV, P., KRÖGER, T., LAMBIEL, C., LANCKMAN, J.-P., LUO, D., MALKOVA, G., MEIKLEJOHN, I., MOSKALENKO, N., OLIVA, M., PHILLIPS, M., RAMOS, M., SANNEL, A. B. K., SERGEEV, D., SEYBOLD, C., SKRYABIN, P., VASILIEV, A., WU, Q., YOSHIKAWA, K., ZHELEZNYAK, M. & LANTUIT, H. 2019. Permafrost is warming at a global scale. *Nature Communications,* 10**,** 264.

BREIMAN, L. 2001. Random forests. *Machine learning,* 45**,** 5-32.

BROOKER, A., FRASER, R. H., OLTHOF, I., KOKELJ, S. V. & LACELLE, D. 2014. Mapping the Activity and Evolution of Retrogressive Thaw Slumps by Tasselled Cap Trend Analysis of a Landsat Satellite Image Stack. *Permafrost and Periglacial Processes,* 25**,** 243-256.

BUNTING, P., CLEWLEY, D., LUCAS, R. M. & GILLINGHAM, S. 2014. The remote sensing and GIS software library (RSGISLib). *Computers & geosciences,* 62**,** 216-226.

BURN, C. & FRIELE, P. 1989. Geomorphology, vegetation succession, soil characteristics and permafrost in retrogressive thaw slumps near Mayo, Yukon Territory. *Arctic***,** 31-40.

BURN, C. R. 2013. PERMAFROST AND PERIGLACIAL FEATURES | Thermokarst Topography. *In:* ELIAS, S. A. & MOCK, C. J. (eds.) *Encyclopedia of Quaternary Science (Second Edition).* Amsterdam: Elsevier.

CHRISTIANSEN, H. H., ETZELMÜLLER, B., ISAKSEN, K., JULIUSSEN, H., FARBROT, H., HUMLUM, O., JOHANSSON, M., INGEMAN-NIELSEN, T., KRISTENSEN, L., HJORT, J., HOLMLUND, P., SANNEL, A. B. K., SIGSGAARD, C., ÅKERMAN, H. J., FOGED, N., BLIKRA, L. H., PERNOSKY, M. A. & ØDEGÅRD, R. S. 2010. The thermal state of permafrost in the nordic area during the international polar year 2007–2009. *Permafrost and Periglacial Processes,* 21**,** 156-181.

COOLEY, W. S., SMITH, C. L., STEPAN, L. & MASCARO, J. 2017. Tracking Dynamic Northern Surface Water Changes with High-Frequency Planet CubeSat Imagery. *Remote Sensing,* 9.

CUNLIFFE, A. M., TANSKI, G., RADOSAVLJEVIC, B., PALMER, W. F., SACHS, T., LANTUIT, H., KERBY, J. T. & MYERS-SMITH, I. H. 2019. Rapid retreat of permafrost coastline observed with aerial drone photogrammetry. *The Cryosphere,* 13**,** 1513-1528.

CZUDEK, T. & DEMEK, J. 1970. Thermokarst in Siberia and its influence on the development of lowland relief. *Quaternary Research,* 1**,** 103-120.

DE MARCHI, D., BURGER, A., KEMPENEERS, P. & SOILLE, P. 2017. Interactive visualisation and analysis of geospatial data with Jupyter. *Proc. of the BiDS,* 17**,** 71-74.

DESYATKIN, R., FEDOROV, A., DESYATKIN, A. & KONSTANTINOV, P. 2015. AIR TEMPERATURE CHANGES AND THEIR IMPACT ON PERMAFROST ECOSYSTEMS IN EASTERN SIBERIA. *Thermal Science,* 19**,** S351-S360.

DETHLOFF, K., HANDORF, D., JAISER, R., RINKE, A. & KLINGHAMMER, P. 2019. Dynamical mechanisms of Arctic amplification. *Annals of the New York Academy of Sciences,* 1436**,** 184-194.

DU, P., SAMAT, A., WASKE, B., LIU, S. & LI, Z. 2015. Random Forest and Rotation Forest for fully polarized SAR image classification using polarimetric and spatial features. *ISPRS Journal of Photogrammetry and Remote Sensing,* 105**,** 38-53.

DUBATH, P., RIMOLDINI, L., SÜVEGES, M., BLOMME, J., LÓPEZ, M., SARRO, L., DE RIDDER, J., CUYPERS, J., GUY, L. & LECOEUR, I. 2011. Random forest automated supervised classification of Hipparcos periodic variable stars. *Monthly Notices of the Royal Astronomical Society,* 414**,** 2602-2617.

EDWARDS, M., GROSSE, G., JONES, B. M. & MCDOWELL, P. 2016. The evolution of a thermokarst-lake landscape: Late Quaternary permafrost degradation and stabilization in interior Alaska. *Sedimentary Geology,* 340**,** 3-14.

EDWARDS, M. E., HAMILTON, T. D., ELIAS, S. A., BIGELOW, N. H. & KRUMHARDT, A. P. 2003. Interglacial Extension of the Boreal Forest Limit in the Noatak Valley, Northwest Alaska: Evidence from an Exhumed River-Cut Bluff and Debris Apron. *Arctic, Antarctic, and Alpine Research,* 35**,** 460-468.

ESPINDOLA, G., CÂMARA, G., REIS, I., BINS, L. & MONTEIRO, A. 2006. Parameter selection for region-growing image segmentation algorithms using spatial autocorrelation. *International Journal of Remote Sensing,* 27**,** 3035-3040.

FATTAL, R. 2007. Image upsampling via imposed edge statistics. *ACM transactions on graphics (TOG),* 26**,** 95.

FOODY, G. M. & MATHUR, A. 2004. Toward intelligent training of supervised image classifications: directing training data acquisition for SVM classification. *Remote Sensing of Environment,* 93**,** 107-117.

FOODY, G. M., MATHUR, A., SANCHEZ-HERNANDEZ, C. & BOYD, D. S. 2006. Training set size requirements for the classification of a specific class. *Remote Sensing of Environment,* 104**,** 1-14.

FOSTER, C., HALLAM, H. & MASON, J. 2015. *Orbit Determination and Differential-drag Control of Planet Labs Cubesat Constellations*.

FREIXENET, J., MUÑOZ, X., RABA, D., MARTÍ, J. & CUFÍ, X. Yet another survey on image segmentation: Region and boundary information integration. European conference on computer vision, 2002. Springer, 408-422.

FRENCH, H. M. 1976. *The periglacial environment,* London, Longman.

GAO, Y. & MAS, J. 2008. *A comparison of the performance of pixel based and object based classifications over images with various spatial resolutions*.

GISLASON, P. O., BENEDIKTSSON, J. A. & SVEINSSON, J. R. Random forest classification of multisource remote sensing and geographic data. IGARSS 2004. 2004 IEEE International Geoscience and Remote Sensing Symposium, 2004. IEEE, 1049-1052.

GISLASON, P. O., BENEDIKTSSON, J. A. & SVEINSSON, J. R. 2006. Random Forests for land cover classification. *Pattern Recognition Letters,* 27**,** 294-300.

GROSSE, G., JONES, B. M. & ARP, C. D. 2013. Thermokarst lakes, drainage, and drained basins. *Treatise on Geomorphology,* 8**,** 325-353.

GU, H., HAN, Y., YANG, Y., LI, H., LIU, Z., SOERGEL, U., BLASCHKE, T. & CUI, S. 2018. *RE: An efficient parallel multi-scale segmentation method for remote sensing imagery.*

GÜNTHER, F., OVERDUIN, P. P., YAKSHINA, I. A., OPEL, T., BARANSKAYA, A. V. & GRIGORIEV, M. N. 2015. Observing Muostakh disappear: permafrost thaw subsidence and erosion of a ground-ice-rich island in response to arctic summer warming and sea ice reduction. *Cryosphere,* 9**,** 151-178.

HAMILTON, T. D. 2001. Quaternary glacial, lacustrine, and fluvial interactions in the western Noatak basin, Northwest Alaska. *Quaternary Science Reviews,* 20**,** 371-391.

HANSEN, J. & LEBEDEFF, S. 1987. Global trends of measured surface air temperature. *Journal of geophysical research: Atmospheres,* 92**,** 13345-13372.

HAWKINS, D. M. 2004. The problem of overfitting. *Journal of chemical information and computer sciences,* 44**,** 1-12.

HINKEL, K. M., EISNER, W. R., BOCKHEIM, J. G., NELSON, F. E., PETERSON, K. M. & DAI, X. 2003. Spatial Extent, Age, and Carbon Stocks in Drained Thaw Lake Basins on the Barrow Peninsula, Alaska. *Arctic, Antarctic, and Alpine Research,* 35**,** 291-300.

HOUBORG, R. & MCCABE, M. F. 2016. High-Resolution NDVI from Planet's Constellation of Earth Observing Nano-Satellites: A New Data Source for Precision Agriculture. *Remote Sensing,* 8**,** 768.

HUANG, L., LIU, L., JIANG, L. & ZHANG, T. 2018. Automatic Mapping of Thermokarst Landforms from Remote Sensing Images Using Deep Learning: A Case Study in the Northeastern Tibetan Plateau. *Remote Sensing,* 10**,** 2067.

IRRGANG, A. M., LANTUIT, H., MANSON, G. K., GÜNTHER, F., GROSSE, G. & OVERDUIN, P. P. 2018. Variability in Rates of Coastal Change Along the Yukon Coast, 1951 to 2015. *Journal of Geophysical Research: Earth Surface,* 123**,** 779-800.

JENSEN, J. R. & JENSEN, R. R. 2013. *Introductory Geographic Information Systems,* Glenview, IL, USA, Pearson Education.

JONES, B. M., ARP, C. D., JORGENSON, M. T., HINKEL, K. M., SCHMUTZ, J. A. & FLINT, P. L. 2009. Increase in the rate and uniformity of coastline erosion in Arctic Alaska. *Geophysical Research Letters,* 36.

JONES, B. M., BULL, D. L., FARQUHARSON, L. M., BAUGHMAN, C. A., ARP, C. D., GROSSE, G., GÜNTHER, F., KANEVSKIY, M., IWAHANA, G., BONDURANT, A. C., BUZARD, R. M., SACHS, T., NITZE, I., KASPER, J. L., FREDERICK, J. M., THOMAS, M., MOTA, A., JONES, C., ROBERTS, J., DALLIMORE, S., TWEEDIE, C., MAIO, C., MANN, D. H., RICHMOND, B., GIBBS, A., XIAO, M. & ROMANOVSKY, V. E. 2018a. High temporal and spatial resolution satellite image observations for the past decade highlight complexities associated with permafrost coastal bluff erosion in the Arctic. *15th International Circumpolar Remote Sensing Symposium.* Potsdam, Germany.

JONES, B. M., FARQUHARSON, L. M., BAUGHMAN, C. A., BUZARD, R. M., ARP, C. D., GROSSE, G., BULL, D. L., GÜNTHER, F., NITZE, I., URBAN, F., KASPER, J. L., FREDERICK, J. M., THOMAS, M., JONES, C., MOTA, A., DALLIMORE, S., TWEEDIE, C., MAIO, C., MANN, D. H., RICHMOND, B., GIBBS, A., XIAO, M., SACHS, T., IWAHANA, G., KANEVSKIY, M. & ROMANOVSKY, V. E. 2018b. A decade of remotely sensed observations highlight complex processes linked to coastal permafrost bluff erosion in the Arctic. *Environmental Research Letters,* 13**,** 115001.

JONES, B. M., HINKEL, K. M., ARP, C. D. & EISNER, W. R. 2008. Modern Erosion Rates and Loss of Coastal Features and Sites, Beaufort Sea Coastline, Alaska. *Arctic,* 61**,** 361-372.

JORGENSON, M. & BROWN, J. 2005. Classification of the Alaskan Beaufort Sea Coast and estimation of carbon and sediment inputs from coastal erosion. *Geo-Marine Letters,* 25**,** 69-80.

JORGENSON, M. T. 2013. 8.20 Thermokarst Terrains. *In:* SHRODER, J. F. (ed.) *Treatise on Geomorphology.* San Diego: Academic Press.

JORGENSON, M. T. & GROSSE, G. 2016. Remote Sensing of Landscape Change in Permafrost Regions. *Permafrost and Periglacial Processes,* 27**,** 324-338.

JORGENSON, M. T., ROMANOVSKY, V., HARDEN, J., SHUR, Y., O'DONNELL, J., SCHUUR, E. A., KANEVSKIY, M. & MARCHENKO, S. 2010. Resilience and vulnerability of permafrost to climate change. *Canadian Journal of Forest Research,* 40**,** 1219-1236.

JORGENSON, M. T. & SHUR, Y. 2007. *Evolution of lakes and basins in northern Alaska and discussion of the thaw lake cycle*.

JORGENSON, M. T., YOSHIKAWA, K., KAVESKY, M., SHUR, Y., ROMANOVSKY, V. E., MARCHENKO, S. S., GROSSE, G., BROWN, J. & JONES, B. M. 2008. Permafrost characteristics of Alaska. *Proceedings of the 9th International Conference on Permafrost, Fairbanks, Alaska, Extended Abstracts***,** 121-122.

JUMAAT, A. K. & KE, C. 2019. A Reformulated Convex and Selective Variational Image Segmentation Model and its Fast Multilevel Algorithm. *Numerical Mathematics: Theory, Methods & Applications,* 12**,** 403-437.

KÄÄB, A., ALTENA, B. & MASCARO, J. 2017. Coseismic displacements of the 14 November 2016 Mw 7.8 Kaikoura, New Zealand, earthquake using the Planet optical cubesat constellation. *Nat. Hazards Earth Syst. Sci.,* 17**,** 627-639.

KÄÄB, A. & HAEBERLI, W. 2001. Evolution of a high-mountain thermokarst lake in the Swiss Alps. *Arctic, Antarctic, and Alpine Research,* 33**,** 385-390.

KAMDI, S. & KRISHNA, R. 2012. Image segmentation and region growing algorithm. *International Journal of Computer Technology and Electronics Engineering (IJCTEE),* 2.

KESSLER, M. A., PLUG, L. J. & WALTER ANTHONY, K. M. 2012. Simulating the decadal- to millennial-scale dynamics of morphology and sequestered carbon mobilization of two thermokarst lakes in NW Alaska. *Journal of Geophysical Research: Biogeosciences,* 117.

KITTEL, T. G. F., BAKER, B. B., HIGGINS, J. V. & HANEY, J. C. 2011. Climate vulnerability of ecosystems and landscapes on Alaska's North Slope. *Regional Environmental Change,* 11**,** 249-264.

KLING, G. W., KIPPHUT, G. W. & MILLER, M. C. 1991. Arctic lakes and streams as gas conduits to the atmosphere: implications for tundra carbon budgets. *Science, New Series,* 251**,** 298-301.

KLUYVER, T., RAGAN-KELLEY, B., PÉREZ, F., GRANGER, B. E., BUSSONNIER, M., FREDERIC, J., KELLEY, K., HAMRICK, J. B., GROUT, J. & CORLAY, S. Jupyter Notebooks-a publishing format for reproducible computational workflows. ELPUB, 2016. 87-90.

KOKELJ, S., LANTZ, T., KANIGAN, J., SMITH, S. & COUTTS, R. 2009. Origin and polycyclic behaviour of tundra thaw slumps, Mackenzie Delta region, Northwest Territories, Canada. *Permafrost and Periglacial Processes,* 20**,** 173-184.

KOKELJ, S., TUNNICLIFFE, J., LACELLE, D., LANTZ, T. & FRASER, R. 2015. *Retrogressive thaw slumps: From slope process to the landscape sensitivity of northwestern Canada*.

KWANG-YUL, K., HAMLINGTON, B. D., HANNA, N. & JINJU, K. 2016. Mechanism of seasonal Arctic sea ice evolution and Arctic amplification. *Cryosphere,* 10**,** 2191-2202.

LACELLE, D., BJORNSON, J. & LAURIOL, B. 2010. Climatic and geomorphic factors affecting contemporary (1950–2004) activity of retrogressive thaw slumps on the Aklavik Plateau, Richardson Mountains, NWT, Canada. *Permafrost and Periglacial Processes,* 21**,** 1-15.

LACELLE, D., BROOKER, A., FRASER, R. H. & KOKELJ, S. V. 2015. Distribution and growth of thaw slumps in the Richardson Mountains–Peel Plateau region, northwestern Canada. *Geomorphology,* 235**,** 40-51.

LANTUIT, H. & POLLARD, W. H. 2008. Fifty years of coastal erosion and retrogressive thaw slump activity on Herschel Island, southern Beaufort Sea, Yukon Territory, Canada. *Geomorphology,* 95**,** 84-102.

LANTUIT, H., POLLARD, W. H., COUTURE, N., FRITZ, M., SCHIRRMEISTER, L., MEYER, H. & HUBBERTEN, H. W. 2012. Modern and Late Holocene Retrogressive Thaw Slump Activity on the Yukon Coastal Plain and Herschel Island, Yukon Territory, Canada. *Permafrost and Periglacial Processes,* 23**,** 39-51.

LANTZ, T. C. & KOKELJ, S. V. 2008. Increasing rates of retrogressive thaw slump activity in the Mackenzie Delta region, N.W.T., Canada. *Geophysical Research Letters,* 35.

LEHNER, B. & DÖLL, P. 2004. Development and validation of a global database of lakes, reservoirs and wetlands. *Journal of Hydrology,* 296**,** 1-22.

LENZ, J., GROSSE, G., JONES, B. M., WALTER ANTHONY, K. M., BOBROV, A., WULF, S. & WETTERICH, S. 2016. Mid-Wisconsin to Holocene Permafrost and Landscape Dynamics based on a Drained Lake Basin Core from the Northern Seward Peninsula, Northwest Alaska. *Permafrost and Periglacial Processes,* 27**,** 56-75.

LEONARD, L., MILES, B., HEIDARI, B., LIN, L., CASTRONOVA, A. M., MINSKER, B., LEE, J., SCAIFE, C. & BAND, L. E. 2019. Development of a participatory Green Infrastructure design, visualization and evaluation system in a cloud supported jupyter notebook computing environment. *Environmental Modelling & Software,* 111**,** 121-133.

LINDGREN, A., HUGELIUS, G., KUHRY, P., CHRISTENSEN, T. R. & VANDENBERGHE, J. 2016. GIS-based Maps and Area Estimates of Northern Hemisphere Permafrost Extent during the Last Glacial Maximum. *Permafrost and Periglacial Processes,* 27**,** 6-16.

M. SOUSA, P. F. & ÅBERG, K. M. 2018. Can we beat overfitting?—A closer look at Cloarec's PLS algorithm. *Journal of Chemometrics,* 32**,** e3002.

MALONE, L., LACELLE, D., KOKELJ, S. & CLARK, I. 2013. *Impacts of hillslope thaw slumps on the geochemistry of permafrost catchments (Stony Creek watershed, NWT, Canada)*.

MARS, J. C. & HOUSEKNECHT, D. W. 2007. Quantitative remote sensing study indicates doubling of coastal erosion rate in past 50 yr along a segment of the Arctic coast of Alaska. [Boulder, CO] :: The Geological Society of America.

MCCABE, M. F., ARAGON, B., HOUBORG, R. & MASCARO, J. 2017. CubeSats in Hydrology: Ultrahigh-Resolution Insights Into Vegetation Dynamics and Terrestrial Evaporation. *Water Resources Research,* 53**,** 10017-10024.

MILLAR, S. 2013. 8.23 Mass Movement Processes in the Periglacial Environment. *In:* SHRODER, J. F. (ed.) *Treatise on Geomorphology.* San Diego: Academic Press.

MILLARD, K. & RICHARDSON, M. 2015. On the Importance of Training Data Sample Selection in Random Forest Image Classification: A Case Study in Peatland Ecosystem Mapping. *Remote Sensing, 7,* 8489-8515.

MORGENSTERN, A., GROSSE, G., GÜNTHER, F., FEDOROVA, I. & SCHIRRMEISTER, L. 2011. Spatial analyses of thermokarst lakes and basins in Yedoma landscapes of the Lena Delta. *The Cryosphere, 5,* 849-867.

MORGENSTERN, A., ULRICH, M., GÜNTHER, F., ROESSLER, S., FEDOROVA, I. V., RUDAYA, N. A., WETTERICH, S., BOIKE, J. & SCHIRRMEISTER, L. 2013. Evolution of thermokarst in East Siberian ice-rich permafrost: A case study. *Geomorphology, 201,* 363-379.

MUSTER, S., LANGER, M., ABNIZOVA, A., YOUNG, K. L. & BOIKE, J. 2015. Spatio-temporal sensitivity of MODIS land surface temperature anomalies indicates high potential for large-scale land cover change detection in Arctic permafrost landscapes. *Remote Sensing of Environment, 168,* 1-12.

NAVON, E., MILLER, O. & AVERBUCH, A. 2005. Color image segmentation based on adaptive local thresholds. *Image and Vision Computing, 23,* 69-85.

NITZE, I., GROSSE, G., JONES, M. B., ARP, D. C., ULRICH, M., FEDOROV, A. & VEREMEEVA, A. 2017. Landsat-Based Trend Analysis of Lake Dynamics across Northern Permafrost Regions. *Remote Sensing, 9.*

NOVIKOVA, A., BELOVA, N., BARANSKAYA, A., ALEKSYUTINA, D., MASLAKOV, A., ZELENIN, E., SHABANOVA, N. & OGORODOV, S. 2018. Dynamics of Permafrost Coasts of Baydaratskaya Bay (Kara Sea) Based on Multi-Temporal Remote Sensing Data. *Remote Sensing, 10,* 1481.

OLIPHANT, T. E. 2007. Python for scientific computing. *Computing in Science & Engineering, 9,* 10-20.

OSTERKAMP, T., JORGENSON, M., SCHUUR, E., SHUR, Y., KANEVSKIY, M., VOGEL, J. & TUMSKOY, V. 2009. Physical and ecological changes associated with warming permafrost and thermokarst in interior Alaska. *Permafrost and Periglacial Processes, 20,* 235-256.

OSTERKAMP, T. & ROMANOVSKY, V. 1999. Evidence for warming and thawing of discontinuous permafrost in Alaska. *Permafrost and Periglacial Processes, 10,* 17-37.

OSTERKAMP, T. E. 2005. The recent warming of permafrost in Alaska. *Global and Planetary Change, 49,* 187-202.

PAL, M. 2005. Random forest classifier for remote sensing classification. *International Journal of Remote Sensing, 26,* 217-222.

PANDA, S., ROMANOVSKY, V. & MARCHENKO, S. 2016. *High-Resolution Permafrost Modeling in the Arctic Network National Parks, Preserves and Monuments*.

PEDREGOSA, F., VAROQUAUX, G., GRAMFORT, A., MICHEL, V., THIRION, B., GRISEL, O., BLONDEL, M., PRETTENHOFER, P., WEISS, R. & DUBOURG, V. 2011. Scikit-learn: Machine learning in Python. *Journal of machine learning research, 12,* 2825-2830.

PEREZ, F., GRANGER, B. E. & HUNTER, J. D. 2010. Python: an ecosystem for scientific computing. *Computing in Science & Engineering,* 13**,** 13-21.

PESTRYAKOVA, L. A., HERZSCHUH, U., WETTERICH, S. & ULRICH, M. 2012. Present-day variability and Holocene dynamics of permafrost-affected lakes in central Yakutia (Eastern Siberia) inferred from diatom records. *Quaternary Science Reviews,* 51**,** 56-70.

PLANET LABS INC. 2018. Planet Imagery: Product Specifications. Available: https://www.planet.com/products/satellite-imagery/files/Planet_Combined_Imagery_Product_Specs_December2017.pdf.

POGHOSYAN, A. & GOLKAR, A. 2017. CubeSat evolution: Analyzing CubeSat capabilities for conducting science missions. *Progress in Aerospace Sciences,* 88**,** 59-83.

RAVENS, T. M., JONES, B. M., ZHANG, J., ARP, C. D. & SCHMUTZ, J. A. 2012. Process-Based Coastal Erosion Modeling for Drew Point, North Slope, Alaska. *Journal of Waterway, Port, Coastal & Ocean Engineering,* 138**,** 122-131.

RODRIGUEZ-GALIANO, V. F., GHIMIRE, B., ROGAN, J., CHICA-OLMO, M. & RIGOL-SANCHEZ, J. P. 2012. An assessment of the effectiveness of a random forest classifier for land-cover classification. *ISPRS Journal of Photogrammetry and Remote Sensing,* 67**,** 93-104.

ROMANOVSKII, N. N., HUBBERTEN, H. W., GAVRILOV, A. V., TUMSKOY, V. E. & KHOLODOV, A. L. 2004. Permafrost of the east Siberian Arctic shelf and coastal lowlands. *Quaternary Science Reviews,* 23**,** 1359-1369.

ROMANOVSKY, V. E., DROZDOV, D. S., OBERMAN, N. G., MALKOVA, G. V., KHOLODOV, A. L., MARCHENKO, S. S., MOSKALENKO, N. G., SERGEEV, D. O., UKRAINTSEVA, N. G., ABRAMOV, A. A., GILICHINSKY, D. A. & VASILIEV, A. A. 2010. Thermal state of permafrost in Russia. *Permafrost and Periglacial Processes,* 21**,** 136-155.

SAADAT, H., ADAMOWSKI, J., BONNELL, R., SHARIFI, F., NAMDAR, M. & ALE-EBRAHIM, S. 2011. Land use and land cover classification over a large area in Iran based on single date analysis of satellite imagery. *ISPRS Journal of Photogrammetry and Remote Sensing,* 66**,** 608-619.

SANTILLI, G., VENDITTOZZI, C., CAPPELLETTI, C., BATTISTINI, S. & GESSINI, P. 2018. CubeSat constellations for disaster management in remote areas. *Acta Astronautica,* 145**,** 11-17.

SCHNEIDER, P. & HOOK, S. J. 2010. Space observations of inland water bodies show rapid surface warming since 1985. *Geophysical Research Letters,* 37.

SCHOWENGERDT, R. A. 1997. CHAPTER 9 - Thematic Classification. *In:* SCHOWENGERDT, R. A. (ed.) *Remote Sensing (Second Edition).* Boston: Academic Press.

SÉJOURNÉ, A., COSTARD, F., FEDOROV, A., GARGANI, J., SKORVE, J., MASSÉ, M. & MÈGE, D. 2015. Evolution of the banks of thermokarst lakes in Central Yakutia (Central Siberia) due to retrogressive thaw slump activity controlled by insolation. *Geomorphology,* 241**,** 31-40.

SERREZE, M. C. & BARRY, R. G. 2011. Processes and impacts of Arctic amplification: A research synthesis. *Global and Planetary Change,* 77**,** 85-96.

SHI, Y., NIU, F., YANG, C., CHE, T., LIN, Z. & LUO, J. 2018. Permafrost Presence/Absence Mapping of the Qinghai-Tibet Plateau Based on Multi-Source Remote Sensing Data. *Remote Sensing,* 10**,** 309.

SHIKLOMANOV, N. I. & NELSON, F. E. 2013. 8.22 Thermokarst and Civil Infrastructure. *In:* SHRODER, J. F. (ed.) *Treatise on Geomorphology.* San Diego: Academic Press.

SMITH, L., SHENG, Y., MACDONALD, G. & HINZMAN, L. 2005. *Disappearing Arctic Lakes. Science 308:1429*.

SMITH, L. C., SHENG, Y. & MACDONALD, G. M. 2007. A first pan-Arctic assessment of the influence of glaciation, permafrost, topography and peatlands on northern hemisphere lake distribution. *Permafrost and Periglacial Processes,* 18**,** 201-208.

SMITH, S. L., ROMANOVSKY, V. E., LEWKOWICZ, A. G., BURN, C. R., ALLARD, M., CLOW, G. D., YOSHIKAWA, K. & THROOP, J. 2010. Thermal state of permafrost in North America: a contribution to the international polar year. *Permafrost and Periglacial Processes,* 21**,** 117-135.

SWANSON, D. & NOLAN, M. 2018. *Growth of Retrogressive Thaw Slumps in the Noatak Valley, Alaska, 2010–2016, Measured by Airborne Photogrammetry*.

TARASENKO, T. V. 2013. Interannual variations in the areas of thermokarst lakes in Central Yakutia. *Water Resources,* 40**,** 111-119.

TILTON, J. C. & LAWRENCE, W. T. Interactive analysis of hierarchical image segmentation. IGARSS 2000. IEEE 2000 International Geoscience and Remote Sensing Symposium. Taking the Pulse of the Planet: The Role of Remote Sensing in Managing the Environment. Proceedings (Cat. No. 00CH37120), 2000. IEEE, 733-735.

ULRICH, M., MATTHES, H., SCHIRRMEISTER, L., SCHÜTZE, J., PARK, H., IIJIMA, Y. & FEDOROV, A. N. 2017a. Differences in behavior and distribution of permafrost-related lakes in Central Yakutia and their response to climatic drivers. *Water Resources Research,* 53**,** 1167-1188.

ULRICH, M., WETTERICH, S., RUDAYA, N., FROLOVA, L., SCHMIDT, J., SIEGERT, C., FEDOROV, A. N. & ZIELHOFER, C. 2017b. Rapid thermokarst evolution during the mid-Holocene in Central Yakutia, Russia. *The Holocene,* 27**,** 1899-1913.

VAN EVERDINGEN, R. 1998. *Multi-language glossary of permafrost and related ground-ice terms in chinese, english, french, german*, Arctic Inst. of North America University of Calgary.

WALTER, K. M., EDWARDS, M. E., GROSSE, G., ZIMOV, S. & CHAPIN, F. 2007. Thermokarst lakes as a source of atmospheric CH4 during the last deglaciation. *science,* 318**,** 633-636.

WANG, Y., SUN, Z. & SUN, Y. 2018. Effects of a thaw slump on active layer in permafrost regions with the comparison of effects of thermokarst lakes on the Qinghai–Tibet Plateau, China. *Geoderma,* 314**,** 47-57.

WOBUS, C., ANDERSON, R., OVEREEM, I., MATELL, N., CLOW, G. & URBAN, F. 2011. Thermal Erosion of a Permafrost Coastline: Improving Process-Based Models Using Time-Lapse Photography. *Arctic, Antarctic, and Alpine Research,* 43**,** 474-484.

XIAOYUE, F., YANCHUN, L., XIAOHU, S., DONG, X., XU, W. & RENCHU, G. 2017. Overfitting Reduction of Text Classification Based on AdaBELM. *Entropy,* 19**,** 330.

XU, M., WATANACHATURAPORN, P., VARSHNEY, P. K. & ARORA, M. K. 2005. Decision tree regression for soft classification of remote sensing data. *Remote Sensing of Environment,* 97**,** 322-336.

YIN, D., LIU, Y., PADMANABHAN, A., TERSTRIEP, J., RUSH, J. & WANG, S. A CyberGIS-Jupyter framework for geospatial analytics at scale. Proceedings of the Practice and Experience in Advanced Research Computing 2017 on Sustainability, Success and Impact, 2017. ACM, 18.

ZAKHAROVA, E. A., KOURAEV, A. V., STEPHANE, G., FRANCK, G., DESYATKIN, R. V. & DESYATKIN, A. R. 2018. Recent dynamics of hydro-ecosystems in thermokarst depressions in Central Siberia from satellite and in situ observations: Importance for agriculture and human life. *Science of The Total Environment,* 615**,** 1290-1304.

ZHANG, T., HEGINBOTTOM, J., BARRY, R. G. & BROWN, J. 2000. Further statistics on the distribution of permafrost and ground ice in the Northern Hemisphere. *Polar geography,* 24**,** 126-131.

ZHANG, X., LI, X. & FENG, Y. 2015. A medical image segmentation algorithm based on bi-directional region growing. *Optik,* 126**,** 2398-2404.

ZHANG, X. M., HE, G. J., ZHANG, Z. M., PENG, Y. & LONG, T. F. 2017. Spectral-spatial multi-feature classification of remote sensing big data based on a random forest classifier for land cover mapping. *Cluster Computing,* 20**,** 2311-2321.

ZIMOV, S. A. E., VOROPAEV, Y. V., SEMILETOV, I., DAVIDOV, S., PROSIANNIKOV, S., CHAPIN, F., CHAPIN, M., TRUMBORE, S. & TYLER, S. 1997. North Siberian lakes: a methane source fueled by Pleistocene carbon. *Science,* 277**,** 800-802.

8. Annex

Used Planet image files

Drew Point 2017	image file
2017-06-28	2017_06_28.tif
2017-07-28	2017_07_28.tiff
2017-09-27	2017_09_27.tiff

Drew Point 2018	image file
2018-07-13	1563684_0571814_2018-07-13_0f49_BGRN_Analytic.tif
	1563684_0571813_2018-07-13_0f49_BGRN_Analytic.tif
2018-08-12	1626337_0571813_2018-08-12_1051_BGRN_Analytic.tif
2018-09-26	1726447_0571813_2018-09-26_1032_BGRN_Analytic.tif
	1726052_0571814_2018-09-26_1008_BGRN_Analytic.tif
2018-10-05	1747381_0571814_2018-10-05_0f35_BGRN_Analytic.tif
	1747390_0571813_2018-10-05_1003_BGRN_Analytic.tif

Yakutia 2017	image file
2017-06-27	582683_5268118_2017-06-27_1036_BGRN_Analytic.tif
2017-07-26	645441_5268118_2017-07-26_0f10_BGRN_Analytic.tf
2017-08-15	690594_5268118_2017-08-15_100c_BGRN_Analytic.tif
2017-09-12	748364_5268118_2017-09-12_1002_BGRN_Analytic.tif
Yakutia 2018	image file
2018-06-06	1483375_5268118_2018-06-06_0e20_BGRN_Analytic.tif
2018-07-08	1551346_5268118_2018-07-08_0f43_BGRN_Analytic.tif
2018-08-04	1607562_5268118_2018-08-04_100c_BGRN_Analytic.tif
2018-09-30	1733822_5268118_2018-09-30_1013_BGRN_Analytic.tif

Noatak 2017	image file
2017-06-12	546912_0470418_2017-06-12_101e_BGRN_Analytic.tif
	546912_0470419_2017-06-12_101e_BGRN_Analytic.tif
	546912_0470518_2017-06-12_101e_BGRN_Analytic.tif
2017-07-26	647876_0470418_2017-07-26_1008_BGRN_Analytic.tif
	647876_0470419_2017-07-26_1008_BGRN_Analytic.tif
	647876_0470519_2017-07-26_1008_BGRN_Analytic.tif
	647876_0470518_2017-07-26_1008_BGRN_Analytic.tif
2017-09-05	735581_0470418_2017-09-05_1010_BGRN_Analytic.tif
	735581_0470518_2017-09-05_1010_BGRN_Analytic.tif
	735841_0470418_2017-09-05_1023_BGRN_Analytic.tif
	735841_0470419_2017-09-05_1023_BGRN_Analytic.tif
2017-09-24	794644_0470419_2017-09-24_1025_BGRN_Analytic.tif
	797784_0470418_2017-09-24_1005_BGRN_Analytic.tif
	797784_0470518_2017-09-24_1005_BGRN_Analytic.tif
Noatak 2018	image file
2018-06-08	1489205_0470419_2018-06-08_0f1b_BGRN_Analytic.tif
	1489961_0470418_2018-06-08_1010_BGRN_Analytic.tif
	1489961_0470518_2018-06-08_1010_BGRN_Analytic.tif
2018-08-13	1628263_0470418_2018-08-13_1006_BGRN_Analytic.tif
	1628263_0470518_2018-08-13_1006_BGRN_Analytic.tif
	1628526_0470419_2018-08-13_1040_BGRN_Analytic.tif
	1628526_0470519_2018-08-13_1040_BGRN_Analytic.tif
2018-09-07	1684176_0470518_2018-09-07_1038_BGRN_Analytic.tif
	1684240_0470418_2018-09-07_1027_BGRN_Analytic.tif
	1684240_0470519_2018-09-07_1027_BGRN_Analytic.tif
	1684812_0470419_2018-09-07_1042_BGRN_Analytic.tif
2018-10-05	1747381_0470418_2018-10-05_0f35_BGRN_Analytic.tif
	1747381_0470419_2018-10-05_0f35_BGRN_Analytic.tif
	1747381_0470518_2018-10-05_0f35_BGRN_Analytic.tif
	1747381_0470519_2018-10-05_0f35_BGRN_Analytic.tif

For further information about the methodology or the data, please contact the author directly.

The amount of data exceeds more than 310GB, as uploading all the data to a cloud would be too complex.